Filter Design for Generalized Frequency-Division Multiplexing

Seungyul Han, *Student Member, IEEE*, Youngchul Sung, *Senior Member, IEEE*, and Yong H. Lee, *Senior Member, IEEE*

***Abstract*—In this paper, optimal filter design for generalized frequency-division multiplexing (GFDM) is considered under two design criteria: rate maximization and out-of-band (OOB) emission minimization. First, the problem of GFDM filter optimization for rate maximization is formulated by expressing the transmission rate of GFDM as a function of GFDM filter coefficients. It is shown that Dirichlet filters are rate-optimal in additive white Gaussian noise channels with no carrier frequency offset (CFO) under linear zero-forcing (ZF) or minimum mean-square error (MMSE) receivers, but in general channels perturbed by CFO a properly designed nontrivial GFDM filter can yield better performance than Dirichlet filters by adjusting the subcarrier waveform to cope with the channel-induced CFO. Next, the problem of GFDM filter design for OOB emission minimization is formulated by expressing the power spectral density of the GFDM transmit signal as a function of GFDM filter coefficients, and it is shown that the OOB emission can be reduced significantly by designing the GFDM filter properly and there is a tradeoff between the transmission rate and OOB radiation for GFDM with linear receivers. Finally, joint design of GFDM filter and window for the two design criteria is considered.**

***Index Terms*—Generalized frequency-division multiplexing, waveform design, filter design, dirichlet filter, single-carrier frequency-division multiplexing.**

I. Introduction

RECENTLY active research is on-going regarding waveform design for 5G wireless communication beyond orthogonal frequency-division multiplexing (OFDM) which has been used for 4G [1]. The main drive for the design of a new waveform is Internet-Of-Things (IoT) applications and machine-type communication (MTC) in 5G, where many low-cost sensors and devices transmit their information with rough synchronization (or possibly asynchronously) to data collecting centers through 5G networks. Thus, a new waveform that has low latency and low OOB emission and is robust against CFO and timing offset (TO) is necessary. Among multi-carrier (MC)-based waveforms beyond OFDM, there are Filter-Bank MC (FBMC), Universal Filtered MC (UFMC), GFDM and so on as candidates for the 5G new waveform to meet such requirements [1]. FBMC can have low OOB emission and robustness against TO and CFO by designing a long prototype filter extending over multiple symbol intervals based on Heisenberg's uncertainty principle [2]–[6], but it has long delay and should have receiver equalization instead of simply adding cyclic prefix (CP) to cope with channel's delay spread. On the other hand, UFMC [7], [8] and GFDM [9]–[12] respectively perform subband filtering and circular convolution filtering within one symbol to achieve such goals. Thus, they have the advantage of low delay, and equalization can be avoided by simply attaching a CP to each symbol since processing is contained within one symbol. Especially, GFDM is an extension of single-carrier frequency-division multiplexing (SC-FDM) used for 4G uplink and has an additional advantage of low peak-to-average-power ratio (PAPR) due to its subsymbol structure. There has been a line of research on GFDM regarding its performance and implementation with several candidate filters such as raised-cosine (RC), Gaussian or Xia filters for GFDM filters [9]–[12]. However, optimal GFDM filters have not been obtained. In this paper, we consider GFDM and provide a systematic framework for optimal filter design for GFDM based on a rigorous rate analysis for GFDM under several receivers including linear matched-filter (MF), ZF and MMSE receivers.

Contributions and Notations: The contributions of this paper are summarized as follows:

- A rigorous rate analysis on GFDM systems is provided and the transmission rate is derived as an explicit function of GFDM filter coefficients in the AWGN channel case. It is shown that in AWGN channels with no CFO, Dirichlet filters are rate-optimal under linear ZF or MMSE receivers.
- The OOB radiation minimization problem under a rate loss constraint is formulated, and it is shown that significant OOB emission reduction can be achieved without rate loss by designing the GFDM filter properly if nonlinear successive interference cancellation (SIC) is assumed at the receiver.
- A framework for GFDM filter design for rate maximization in uplink GFDM networks perturbed by CFO is presented and it is shown that proper GFDM filtering can yield better rate performance than Dirichlet filters in this case.

Manuscript received July 6, 2016; revised November 6, 2016; accepted December 2, 2016. Date of publication December 19, 2016; date of current version January 26, 2017. The associate editor coordinating the review of this manuscript and approving it for publication was Dr. Itsik Bergel. This work was supported by the Basic Science Research Program through the National Research Foundation of Korea (NRF) funded by the Ministry of Education under Grant 2013R1A1A2A10060852.

The authors are with Department of Electrical Engineering, Korea Advanced Institute of Science and Technology, Daejeon 305-701, South Korea (e-mail: sy.han@kaist.ac.kr; ysung@ee.kaist.ac.kr; yohlee@kaist.ac.kr).

Color versions of one or more of the figures in this paper are available online at http://ieeexplore.ieee.org.

Digital Object Identifier 10.1109/TSP.2016.2641382

TABLE I
TABLE OF NOTATIONS

$\mathbf{A}^T$	=	The transpose of matrix $\mathbf{A}$.
$\mathbf{A}^*$	=	The complex conjugate of matrix $\mathbf{A}$.
$\mathbf{A}^H$	=	The conjugate transpose of matrix $\mathbf{A}$.
$[\mathbf{A}]_{i,j}$	=	The (i,j)-th element of matrix $\mathbf{A}$.
$\mathbf{A}(:,k)$	=	The k-th column of matrix $\mathbf{A}$.
$\mathrm{diag}(\mathbf{A}_1,\cdots,\mathbf{A}_n)$	=	The block diagonal matrix with diagonal elements $\mathbf{A}_1,\cdots,\mathbf{A}_n$.
$\mathbf{I}_n$	=	The identity matrix of size n.
$\mathbf{1}_n$	=	The column vector of size n whose entries are all one.
$\mathbf{0}_{m\times n}$	=	The $m\times n$ matrix whose entries are all zero. Size is omitted if unnecessary.
ι	=	$\sqrt{-1}$.
$\mathbf{W}_n$	=	The n-point discrete Fourier transform (DFT) matrix, i.e., $[\mathbf{W}_n]_{i,j} = \frac{1}{\sqrt{n}}e^{-\iota 2\pi ij/n},\ i,j=0,1,\cdots,n-1$.
$\delta_{m,n}$	=	$\begin{cases}1 & \text{if } m=n,\\ 0 & \text{if } m\neq n.\end{cases}$
$\mathcal{CN}(\boldsymbol{\mu},\boldsymbol{\Sigma})$	=	The circularly-symmetric complex Gaussian distribution with mean vector $\boldsymbol{\mu}$ and covariance matrix $\boldsymbol{\Sigma}$.
$\mathbf{X}\sim P$	=	$\mathbf{X}$ is distributed according to the probability distribution P.
$\mathbb{E}\{\mathbf{X}\}$	=	The expectation of $\mathbf{X}$.

- Finally, joint design frameworks of GFDM filter and window are proposed to enhance the performance of GFDM further.

The notations of this paper are summarized in Table I.

II. System Model

We first consider GFDM transmission without windowing by postponing joint design of GFDM filter and window to Section V. Let $\mathbf{s}[i]=[s_0[i],\cdots,s_{N-1}[i]]^T$ be the data vector composed of the N complex data subsymbols $s_0[i],\cdots,s_{N-1}[i]$ carried by the i-th GFDM symbol. Since each symbol processing is independent and identical in GFDM, we consider one symbol time interval with the symbol time index omitted. In GFDM, the data vector $\mathbf{s}$ is decomposed into K subvectors each with size M as

$$\mathbf{s}=[s_0,\cdots,s_{N-1}]^T=[\mathbf{s}_0^T,\cdots,\mathbf{s}_{K-1}^T]^T, \tag{1}$$
$$\mathbf{s}_k=[s_{kM},\cdots,s_{kM+M-1}]^T,\quad k=0,\cdots,K-1,$$

where K is the number of subcarriers and M is the number of subsymbols carried by one subcarrier such that $N=MK$. In GFDM, subvector $\mathbf{s}_k$ is carried by the k-th subcarrier based on time-domain filtering. That is, s_{kM+m} is carried on the m-th subsymbol in the k-th subcarrier with the shaping pulse [9]

$$\tilde{g}_{k,m}[n]=\tilde{g}[n-mK]e^{\iota 2\pi kn/K},\quad n=0,\cdots,N-1, \tag{2}$$

where n is the time sample or chip index, and $\tilde{g}[n-mK]$ is the mK-sample *circularly shifted* version of the time-domain GFDM filter $g[n]$. Thus, the transmit signal of GFDM for one symbol time interval is expressed as [9], [11]

$$x[n]=\sum_{k=0}^{K-1}x_k[n],\quad n=0,1,\cdots,N-1, \tag{3}$$

where $x_k[n]=\sum_{m=0}^{M-1}\tilde{g}_{k,m}[n]s_{kM+m}=\sum_{m=0}^{M-1}\tilde{g}[n-mK]e^{\iota 2\pi kn/K}s_{kM+m}$.

A. The Matrix Transmit Signal Model

The transmit signal (3) can be written in a matrix form as

$$\mathbf{x}=\boldsymbol{\Phi}\mathbf{s}, \tag{4}$$

where $\mathbf{x}=[x[0],\cdots,x[N-1]]^T$ and $\boldsymbol{\Phi}$ is an $N\times N$ matrix given by $[\boldsymbol{\Phi}]_{n,kM+m}=\tilde{g}_{k,m}[n]$. The matrix $\boldsymbol{\Phi}$ can be expressed as the product of several relevant matrices [11]. First, note that $x_k[n]$ in (3) can be rewritten as

$$x_k[n]=\left[\left(\sum_{m=0}^{M-1}\delta[n-mK]\right)\circledast g[n]\right]e^{\iota 2\pi kn/K}s_{kM+m}, \tag{5}$$

where $\circledast$ denotes the N-point circular convolution, and the signal (5) can be rewritten based on the properties of discrete Fourier transform (DFT) as (6) [11], shown at the bottom of the page. Note in (6) that

$$\mathrm{DFT}_N\left(\sum_{m=0}^{M-1}s_k[m]\delta[n-mK]\right)=\frac{1}{\sqrt{K}}\begin{bmatrix}\mathbf{W}_M\mathbf{s}_k\\ \vdots\\ \mathbf{W}_M\mathbf{s}_k\end{bmatrix}\Bigg\}N,$$

$\mathrm{DFT}_N(g[n])$ is the N-point frequency response of the GFDM filter $g[n]$, and convolution with $\mathrm{DFT}_N\left(e^{\iota 2\pi kn/K}\right)$ corresponds to kM-sample circular shift with scaling $\sqrt{N}$ in the frequency domain. Applying the above observations to (6), we can rewrite the GFDM transmit signal (4) as

$$\mathbf{x}=\mathbf{W}_N^H\sum_{k=0}^{K-1}\tilde{\mathbf{P}}_k\tilde{\boldsymbol{\Gamma}}\tilde{\mathbf{R}}\mathbf{W}_M\mathbf{s}_k, \tag{7}$$

where $\tilde{\mathbf{R}}$ is the repetition matrix given by

$$\tilde{\mathbf{R}}=\underbrace{[\mathbf{I}_M,\cdots,\mathbf{I}_M]}_{K}^T,$$

$\tilde{\boldsymbol{\Gamma}}$ is the $N\times N$ diagonal frequency-domain filtering matrix containing $\sqrt{M}\mathrm{DFT}_N(g[n])$ as its diagonal elements, and $\tilde{\mathbf{P}}_k$ is the $N\times N$ permutation matrix implementing kM-sample circular shifting [11].

In typical GFDM systems, the frequency response of the pulse shaping filter $g[n]$ is designed to be zero except LM samples. In this case, $\tilde{\mathbf{R}}$, $\tilde{\boldsymbol{\Gamma}}$ and $\tilde{\mathbf{P}}_k$ in (7) can be replaced with

$$\begin{aligned}x_k[n]&=\mathrm{IDFT}_N\left(\mathrm{DFT}_N\left(\left[\left(\sum_{m=0}^{M-1}s_{kM+m}\delta[n-mK]\right)\circledast g[n]\right]e^{\iota 2\pi kn/K}\right)\right)\\&=\mathrm{IDFT}_N\left(\mathrm{DFT}_N\left(\sum_{m=0}^{M-1}s_{kM+m}\delta[n-mK]\right)\cdot\mathrm{DFT}_N(g[n])\circledast\mathrm{DFT}_N\left(e^{\iota 2\pi kn/K}\right)\right).\end{aligned} \tag{6}$$

the reduced-size L times repetition matrix $\mathbf{R}$, the $LM \times LM$ diagonal frequency-domain filtering matrix $\mathbf{\Gamma}$, and the $N \times LM$ permutation matrix $\mathbf{P}_k$, respectively. In the example of a RC or square-root RC (RRC) filter $g[n]$ with a roll-off factor $\alpha \in [0, 1]$, the repetition factor L is two and signal mixing for desired properties by GFDM occurs only with two adjacent subcarriers for each subcarrier [9]. In this paper, we consider the mostly-considered case of $L = 2$ as in [9], [11] from here on. In this case, we have [11]

$$\mathbf{x} = \mathbf{W}_N^H \sum_{k=0}^{K-1} \mathbf{P}_k \mathbf{\Gamma} \mathbf{R} \mathbf{W}_M \mathbf{s}_k, \tag{8}$$

where $\mathbf{R} = [\mathbf{I}_M \, \mathbf{I}_M]^T$, $\mathbf{\Gamma} = \left[\begin{smallmatrix} \mathbf{\Gamma}^{(f)} & \mathbf{0} \\ \mathbf{0} & \mathbf{\Gamma}^{(r)} \end{smallmatrix}\right] = \text{diag}(\gamma_0, \gamma_1, \cdots, \gamma_{2M-1})$, and $\mathbf{P}_k$ is the $N \times 2M$ subcarrier mapping matrix for the k-th subcarrier which is given by

$$\mathbf{P}_k = \begin{bmatrix} \mathbf{0}_M & \cdots & \mathbf{0}_M & \underbrace{\mathbf{I}_M}_{k-\text{th}} & \cdots & \mathbf{0}_M \\ \mathbf{0}_M & \cdots & \mathbf{I}_M & \mathbf{0}_M & \cdots & \mathbf{0}_M \end{bmatrix}^T. \tag{9}$$

Here, $\mathbf{\Gamma}^{(f)}$ and $\mathbf{\Gamma}^{(r)}$ are diagonal matrices with size M, and $\gamma_0, \cdots, \gamma_{2M-1}$ are the *design variables* in GFDM filter design. The data model (8) can further be expressed as

$$\mathbf{x} = \mathbf{W}_N^H \mathbf{P} \text{diag}(\mathbf{F}, \cdots, \mathbf{F}) \mathbf{s}, \tag{10}$$

where

$$\mathbf{P} = [\mathbf{P}_0, \cdots, \mathbf{P}_{K-1}] \text{ and } \mathbf{F} = \mathbf{\Gamma} \mathbf{R} \mathbf{W}_M. \tag{11}$$

Thus, $\mathbf{\Phi}$ in (4) is given by

$$\mathbf{\Phi} = \mathbf{W}_N^H \mathbf{P} \text{diag}(\mathbf{F}, \cdots, \mathbf{F}). \tag{12}$$

Note that GFDM with the repetition factor $L = 1$ subsumes OFDM, single-carrier (SC), and SC-FDM. When $L = 1$, $K = N$, and $M = 1$, the corresponding GFDM is OFDM. When $L = 1$, $K = 1$, and $M = N$, the corresponding GFDM is SC. When $L = 1$, $1 < M < N$, $\mathbf{\Gamma} = \mathbf{I}_M$ (i.e., the filter $g[n]$ is a Dirichlet filter which is the RC filter with roll-off factor $\alpha = 0$), and $\mathbf{P}_k = [\mathbf{0}, \cdots, \mathbf{I}_M, \cdots, \mathbf{0}]^T$, the corresponding GFDM reduces to SC-FDM [9].

We assume that the data subvectors $\mathbf{s}_k$, $k = 0, \cdots, K-1$ are zero-mean independent Gaussian random vectors with $\mathbf{s}_k \sim \mathcal{CN}(\mathbf{0}, P_s \mathbf{I})$, where P_s is the data subsymbol power. Then, the total transmit power P_t of one GFDM symbol is obtained from (8) as

$$P_t = \mathbb{E}\{\text{tr}(\mathbf{x}\mathbf{x}^H)\} = P_s \sum_{k=0}^{K-1} \text{tr}(\mathbf{P}_k \mathbf{\Gamma} \mathbf{R} \mathbf{W}_M \mathbf{W}_M^H \mathbf{R}^H \mathbf{\Gamma}^H \mathbf{P}_k^H)$$

$$= K P_s \sum_{m=1}^{2M-1} |\gamma_m|^2, \tag{13}$$

where the fact that $\mathbf{W}_M \mathbf{W}_M^H = \mathbf{I}$ and $\mathbf{P}_k^H \mathbf{P}_k = \mathbf{I}$ and the structure of $\mathbf{R}$ are used. We set $P_t = N P_s$ to have a normalized filter power constraint

$$\sum_{m=1}^{2M-1} |\gamma_m|^2 = M. \tag{14}$$

B. The Channel and Receiver Model

We assume that a CP of size N_{cp} samples is added to the transmit signal vector $\mathbf{x}$ in (10) in the time domain to yield the CP-added transmit signal $\bar{\mathbf{x}} = [x[N - N_{cp}], \cdots, x[N-1], x[0], \cdots, x[N-1]]^T$. This CP-added signal vector $\bar{\mathbf{x}}$ is transmitted through a multipath fading channel with an N_{cp}-tap finite impulse response (FIR) $\mathbf{h} = [h[0], \cdots, h[N_{cp} - 1]]^T$ and is received at the receiver with AWGN to yield the received signal vector $\bar{\mathbf{y}} = [y[-N_{cp}], \cdots, y[-1], y[0], \cdots, y[N-1]]^T$. At the receiver, the first N_{cp} samples of $\bar{\mathbf{y}}$ corrupted by inter-block interference are removed. Thus, the CP-portion-removed received signal vector $\mathbf{y} = [y[0], \cdots, y[N-1]]^T$ is given by

$$\mathbf{y} = \mathbf{H}\mathbf{x} + \mathbf{n} = \mathbf{H}\mathbf{\Phi}\mathbf{s} + \mathbf{n}, \tag{15}$$

where $\mathbf{H}$ is the $N \times N$ circulant channel matrix with the first column given by $[\mathbf{h}^T \;\; \mathbf{0}^T]^T$, and the noise vector $\mathbf{n} \sim \mathcal{CN}(\mathbf{0}, \sigma_n^2 \mathbf{I})$ with the noise variance σ_n^2.*

We consider standard receivers. In linear receivers, an estimate of the symbol vector for further processing is obtained as $\hat{\mathbf{s}} = \mathbf{L}\mathbf{y}$. The MF receiver $\mathbf{L} = \mathbf{\Phi}^H$ is simple and aims at maximizing the signal-to-noise ratio (SNR) for each subsymbol without considering interference. In the case of OFDM and SC-FDM, the MF receiver $\mathbf{L} = \mathbf{\Phi}^H$ diagonalizes the circulant channel matrix $\mathbf{H}$, since $\mathbf{W}_N \mathbf{H} \mathbf{W}_N^H$ is a diagonal matrix, and separates the subcarrier channels without inter-subcarrier interference. In nontrivial GFDM, however, symbol mixing is made intentionally to achieve certain design goals as seen in (8) with the repetition matrix $\mathbf{R}$ and the summation operation. Thus, the simple MF receiver experiences inter-subcarrier interference and this inter-subcarrier interference limits the performance of the MF receiver in GFDM. To eliminate the inter-subcarrier interference, SIC can be employed on top of the MF receiver for GFDM, or the linear ZF receiver $\mathbf{L} = (\mathbf{H}\mathbf{\Phi})^{-1}$ or the linear MMSE receiver $\mathbf{L} = ((\sigma_n^2/P_s)\mathbf{I}_N + \mathbf{\Phi}^H \mathbf{H}^H \mathbf{H} \mathbf{\Phi})^{-1} \mathbf{\Phi}^H \mathbf{H}^H$ can be used with reduced complexity.

III. Rate Analysis for GFDM in the AWGN Case

In this section, we analyze the rate of GFDM with the receivers considered in Section II-B and derive a rate-optimal GFDM filter for linear ZF or MMSE receivers in the AWGN channel case with no CFO, which is one of the most important channel models in communication.

A. The MF or MF/SIC Receiver Case

The signal estimate of the MF receiver is given by

$$\hat{\mathbf{s}} = \mathbf{\Phi}^H \mathbf{y} = \mathbf{\Phi}^H \mathbf{H} \mathbf{\Phi} \mathbf{s} + \mathbf{\Phi}^H \mathbf{n}. \tag{16}$$

From (10), (12) and (15), the estimated signal vector at the k-th subcarrier can be written as

$$\hat{\mathbf{s}}_k = \mathbf{F}^H \mathbf{P}_k^H \mathbf{\Lambda}_H \mathbf{P} \text{diag}(\mathbf{F}, \cdots, \mathbf{F}) \mathbf{s} + \mathbf{F}^H \mathbf{P}_k^H \mathbf{W}_N \mathbf{n}, \tag{17}$$

*Note that the assumption that the whole vector $\mathbf{x}$, which is the sum of all subcarrier signals, goes through the single channel $\mathbf{h}$ is relevant to point-to-point communication scenarios. An uplink network scenario will be considered later in Section IV-B.

where $\mathbf{\Lambda}_H = \mathbf{W}_N \mathbf{H} \mathbf{W}_N^H$ is the $N \times N$ diagonal matrix whose diagonal elements are the eigenvalues of the circulant channel matrix $\mathbf{H}$.

In the AWGN channel case, we have $\mathbf{H} = \mathbf{I}$ and $\mathbf{y} = \mathbf{\Phi s} + \mathbf{n}$ from (15), and the sum capacity of the data model $\mathbf{y} = \mathbf{\Phi s} + \mathbf{n}$ is given by [13]

$$\sum_{n=0}^{N-1} \log\left(1 + \frac{P_s}{\sigma_n^2}\xi_n^2\right) \le N \log\left(1 + \frac{P_s}{\sigma_n^2}\right) =: R_{max}, \quad (18)$$

where ξ_n is the n-th singular value of the matrix $\mathbf{\Phi}$ and the inequality in (18) is obtained by applying Jensen's inequality to the concave function $f(x) = \log(1+x)$ with the power constraint $P_t = \mathbb{E}\{\mathrm{tr}(\mathbf{x}\mathbf{x}^H)\} = P_s \mathrm{tr}(\mathbf{\Phi}\mathbf{\Phi}^H) = P_s ||\mathbf{\Phi}||_F^2 = P_s \sum_{n=0}^{N-1} \xi_n^2 \le N P_s$, i.e., $\frac{1}{N}\sum_{n=0}^{N-1} \xi_n^2 \le 1$. The upper bound in (18) is achieved when $\xi_0 = \cdots = \xi_{N-1} = 1$, equivalently, $\mathbf{\Phi}^H \mathbf{\Phi} = \mathbf{\Phi}\mathbf{\Phi}^H = \mathbf{I}$, i.e., the full orthonormality among the pulses carrying s_{kM+m}, $m = 0, 1, \cdots, M-1$, $k = 0, 1, \cdots, K-1$ is satisfied. (Note that $[\mathbf{\Phi}]_{n, kM+m} = \tilde{g}_{k,m}[n]$.) (A similar observation was made in [14] for a multiple-input multiple-output (MIMO) context.)

Indeed, if the full orthonormality among the pulses $\tilde{g}_{k,m}[n]$ carrying s_{kM+m}, $m = 0, 1, \cdots, M-1$, $k = 0, 1, \cdots, K-1$ were preserved, then the MF symbol SNR would be given from (16) with $\mathbf{H} = \mathbf{I}$ by $\mathrm{SNR}_{k,m} = \frac{P_s}{\sigma_n^2} \sum_n |\tilde{g}_{k,m}[n]|^2 = \frac{P_s}{\sigma_n^2} \sum_n |g[n]|^2 \overset{(a)}{=} \frac{P_s}{\sigma_n^2} \sum_{l=0}^{M-1} \frac{1}{M} \left(|\gamma_l|^2 + |\gamma_{M+l}|^2\right) \overset{(b)}{=} \frac{P_s}{\sigma_n^2}$, which is the *ideal MF SNR bound*, where step (a) is due to Parseval's theorem and step (b) is due to the filter power constraint (14), and the corresponding sum rate would be given by R_{max} in (18). However, when a non-trivial GFDM filter $\mathbf{\Gamma}$ with $L = 2$ is applied, intentional inter-subcarrier mixing occurs, the orthogonality among $\tilde{g}_{k,m}[n]$ is broken, and inter-subcarrier/inter-subsymbol interference exists. In this case, the signal-to-interference-plus-noise ratio (SINR) for symbol s_{kM+m} degrades from the ideal MF SNR bound and is given in the following theorem.

Theorem 1: Under the AWGN channel $\mathbf{H} = \mathbf{\Lambda}_H = \mathbf{I}_N$ with the transmit power $P_t = NP_s$, the SINR of the m-th subsymbol of the k-th subcarrier in GFDM with the MF receiver is given by

$$\mathrm{SINR}_{k,m}^{MF}(\boldsymbol{\gamma}) = \frac{P_s}{a(\boldsymbol{\gamma})P_s + \sigma_n^2}, \quad (19)$$

where $\boldsymbol{\gamma} = [\gamma_0, \cdots, \gamma_{2M-1}]$, and $a(\boldsymbol{\gamma}) = \frac{1}{M^2}\sum_{p \ne m, p=0}^{M-1} |\sum_{l=0}^{M-1} e^{\iota 2\pi (m-p) l/M} \left(|\gamma_l|^2 + |\gamma_{M+l}|^2\right)|^2 + \frac{2}{M^2}\sum_{p=0}^{M-1} |\sum_{l=0}^{M-1} e^{\iota 2\pi (m-p) l/M} \gamma_l \gamma_{M+l}^*|^2$.

Proof: See Appendix. ■

The sum rate of GFDM with the MF receiver is given by $R_{MF}(\boldsymbol{\gamma}) = \sum_{k=0}^{K-1}\sum_{m=0}^{M-1} \log(1 + \mathrm{SINR}_{k,m}^{MF})$, where $\mathrm{SINR}_{m,k}^{MF}$ is given by (19) and depends on the GFDM filter $\boldsymbol{\gamma}$. With a non-trivial GFDM filter $\boldsymbol{\gamma}$, e.g., the RRC filter with a non-zero roll-off factor [9], the rate performance of the MF receiver for GFDM saturates at high SNR due to the intentional inter-subcarrier interference, as shown in Fig. 3. In order to eliminate the inter-subcarrier interference for the MF receiver, SIC can be applied on top of the MF [9], [12]. Note from Proof of Theorem 1 that the term $a(\boldsymbol{\gamma})P_s$ in the denominator of the right-hand side (RHS) of the $\mathrm{SINR}_{k,m}^{MF}(\boldsymbol{\gamma})$ expression in (19) is the interference from other data subsymbols. Hence, if SIC is performed until the interference is removed, the interference term $a(\boldsymbol{\gamma})P_s$ disappears and the best subsymbol SNR in this case is given by P_s/σ_n^2, yielding the maximum rate R_{max} in (18). (For implementation of SIC in GFDM, see [12].)

Note that in the AWGN case of $\mathbf{H} = \mathbf{I}$, the MF output is given by $\hat{\mathbf{s}} = \mathbf{\Phi}^H \mathbf{y} = \mathbf{\Phi}^H \mathbf{\Phi s} + \mathbf{\Phi}^H \mathbf{n}$ from (16) and the corresponding subsymbol SINR is given by $\mathrm{SINR}_{k,m}^{MF}(\boldsymbol{\gamma}) = \frac{P_s}{a(\boldsymbol{\gamma})P_s + \sigma_n^2}$. Hence, the orthonormality condition $\mathbf{\Phi}^H \mathbf{\Phi} = \mathbf{I}$ to achieve the upper bound in (18) is equivalent to $a(\boldsymbol{\gamma}) = 0$. The explicit necessary and sufficient condition for $a(\boldsymbol{\gamma}) = 0$ is not straightforward to obtain, but a sufficient condition is given by the Dirichlet filter $\gamma_0 = \cdots = \gamma_{M-1} = 1$ and $\gamma_M = \cdots = \gamma_{2M-1} = 0$. We shall discuss this condition in more detail in the next subsection.

B. Maximum Rate Filtering for the ZF or MMSE Receiver

In this section, as an alternative to the MF/SIC receiver, we consider the ZF or MMSE receiver, which eliminates inter-subcarrier and inter-subsymbol interference with simple linear processing, and derive an optimal GFDM filter that maximizes the data rate for GFDM under the ZF or MMSE receiver.

In the case of the ZF receiver, the estimated signal vector is given from (12) and (15) by

$$\begin{aligned}
\begin{bmatrix} \hat{\mathbf{s}}_0 \\ \vdots \\ \hat{\mathbf{s}}_{K-1} \end{bmatrix} &= (\mathbf{H}\mathbf{W}_N^H \mathbf{P} \mathrm{diag}(\mathbf{F}, \cdots, \mathbf{F}))^{-1} \mathbf{y} \\
&= (\mathbf{W}_N^H \mathbf{W}_N \mathbf{H} \mathbf{W}_N^H \mathbf{P} \mathrm{diag}(\mathbf{F}, \cdots, \mathbf{F}))^{-1} \mathbf{y} \\
&= (\mathbf{P}\mathrm{diag}(\mathbf{F}, \cdots, \mathbf{F}))^{-1} \mathbf{\Lambda}_H^{-1} \mathbf{W}_N \mathbf{y} \\
&= \begin{bmatrix} \mathbf{s}_0 \\ \vdots \\ \mathbf{s}_{K-1} \end{bmatrix} + (\mathbf{P}\mathrm{diag}(\mathbf{F}, \cdots, \mathbf{F}))^{-1} \mathbf{\Lambda}_H^{-1} \tilde{\mathbf{n}}, \quad (20)
\end{aligned}$$

where $\tilde{\mathbf{n}} = \mathbf{W}_N \mathbf{n} \sim \mathcal{CN}(\mathbf{0}, \sigma_n^2 \mathbf{I}_N)$.

Remark 1: Note from (20) that the ZF receiver processing can be done efficiently with low complexity. We sequentially apply the N-point DFT to $\mathbf{y}$, multiplication of diagonal $\mathbf{\Lambda}_H^{-1}$, which is simple elementwise scaling, and multiplication of $(\mathbf{P}\mathrm{diag}(\mathbf{F}, \cdots, \mathbf{F}))^{-1}$. The N-point DFT based on fast Fourier transform (FFT) requires $O(N \log N)$ complexity and the multiplication of the diagonal matrix $\mathbf{\Lambda}_H^{-1}$ requires only $O(N)$ complexity. The last step can also be performed with low complexity $O(N \log \max(M, K))$ by reformulating $(\mathbf{P}\mathrm{diag}(\mathbf{F}, \cdots, \mathbf{F}))^{-1}$ with block DFT matrices. Hence, the overall complexity for ZF processing for GFDM is given by $O(N \log N)$. See Proof of Theorem 2 and Remark 2 in Appendix for detail.

In the ZF receiver case, the signal part is completely separated but the noise is enhanced. The noise enhancement reduces the effective channel gain of each separate parallel Gaussian channel provided by ZF processing [15]. The rate of GFDM with the ZF receiver is the sum of the rates of the N parallel Gaussian channels and is given by the following theorem.

Theorem 2: In the general FIR channel case, the sum rate of GFDM with the ZF receiver is given by $R_{ZF}(\boldsymbol{\gamma}) =$

$$M\sum_{k=0}^{K-1}\log\left(1+\frac{P_s/\sigma_n^2}{\sum_{p=0}^{K-1}\sum_{q=0}^{M-1}\left|\sum_{l=0}^{K-1}\frac{c_{k,p,q,l}}{\gamma_q+d_l\gamma_{M+q}}\right|^2}\right), \tag{21}$$

where $c_{k,p,q,l}=\frac{1}{\sqrt{M}}\frac{1}{K}e^{\iota 2\pi(k-p)l/K}[\mathbf{\Lambda}_H^{-1}]_{pM+q,pM+q}$ and $d_l=e^{\iota 2\pi l/K}$. In the AWGN channel case, the sum rate of GFDM with the ZF receiver is given by

$$R_{ZF}(\boldsymbol{\gamma})=N\log\left(1+\frac{P_s/\sigma_n^2}{\frac{1}{N}\sum_{l=0}^{K-1}\sum_{q=0}^{M-1}\frac{1}{|\gamma_q+d_l\gamma_{M+q}|^2}}\right). \tag{22}$$

Proof: See Appendix. ■

Using Theorem 2, we can formulate the problem of finding an optimal GFDM filter to maximize the rate of GFDM with the ZF receiver. In particular, in the AWGN channel case, by exploiting the monotonicity of the logarithm function and the function $f(x)=1/x$ in (22), the optimization problem reduces to the following problem:

Problem 1:

$$\arg\min_{\boldsymbol{\gamma}}\ \sum_{l=0}^{K-1}\sum_{q=0}^{M-1}\frac{1}{|\gamma_q+d_l\gamma_{M+q}|^2}$$
$$\text{s.t.}\ \sum_{m=0}^{2M-1}|\gamma_m|^2=M. \tag{23}$$

Now consider the MMSE receiver case. The MMSE receiver in the AWGN channel case is given by $\mathbf{L}=((\sigma_n^2/P_s)\mathbf{I}+\mathbf{\Phi}^H\mathbf{\Phi})^{-1}\mathbf{\Phi}^H$. In the MMSE receiver case, computing the mutual information $I(\mathbf{s};\hat{\mathbf{s}}=\mathbf{L}\mathbf{y})$, we have the sum rate given by

$$R_{MMSE}(\boldsymbol{\gamma})=\sum_{k=0}^{K-1}\sum_{m=0}^{M-1}\log(1+\rho_{k,m,MMSE}(\boldsymbol{\gamma})), \tag{24}$$

where the effective output SNR for each subchannel is given by [15]

$$\rho_{k,m,MMSE}(\boldsymbol{\gamma})=\frac{P_s/\sigma_n^2}{\left[\left(\mathbf{\Phi}^H\mathbf{\Phi}+\frac{\sigma_n^2}{P_s}\mathbf{I}\right)^{-1}\right]_{kM+m,kM+m}}-1. \tag{25}$$

Based on (24) and (25), the sum rate of GFDM with the MMSE receiver is derived in the following theorem:

Theorem 3: In the AWGN channel case, the sum rate of GFDM with the MMSE receiver is given by

$$R_{MMSE}(\boldsymbol{\gamma})=N\log\left(\frac{P_s/\sigma_n^2}{D(\boldsymbol{\gamma})}\right), \tag{26}$$

where $D(\boldsymbol{\gamma})=\frac{1}{N}\sum_{l=0}^{K-1}\sum_{q=0}^{M-1}\frac{1}{|\gamma_q+d_l\gamma_{M+q}|^2+\sigma_n^2/P_s}$.

Proof: See Appendix. ■

In a similar way to the ZF case, the problem of filter optimization for GFDM with the MMSE receiver in the AWGN channel case is formulated based on Theorem 3 as follows:

Problem 2:

$$\arg\min_{\boldsymbol{\gamma}}\ \sum_{l=0}^{K-1}\sum_{q=0}^{M-1}\frac{1}{|\gamma_q+d_l\gamma_{M+q}|^2+\sigma_n^2/P_s}$$
$$\text{s.t.}\ \sum_{m=0}^{2M-1}|\gamma_m|^2=M. \tag{27}$$

Solutions to Problems 1 and 2 are given by the following theorem.

Theorem 4: In the AWGN channel case, the Dirichlet filter (i.e., $\gamma_0=\cdots=\gamma_{M-1}=1$ and $\gamma_M=\cdots=\gamma_{2M-1}=0$) maximizes the sum rate for GFDM with the ZF or MMSE receiver, and the corresponding rate is given by $N\log(1+\frac{P_s}{\sigma_n^2})$. Furthermore, any filter cannot have a larger rate than the Dirichlet filter for GFDM with the ZF or MMSE receiver.

Proof: See Appendix ■.

As seen in Section III-A, with the nonlinear MF/SIC receiver, any filter satisfying the power constraint is rate-optimal for GFDM under the assumption of ideal SIC in the AWGN channel case. However, Theorem 4 states that with the linear ZF or MMSE receiver, the Dirichlet filter, i.e., SC-FDM with no intentional inter-subcarrier mixing, is rate-optimal for GFDM, and the achievable rate is identical to the sum capacity upper bound, R_{max} in (18). In the example of an RRC filter with a non-zero roll-off factor [9], the sum rate loss occurs with a linear receiver, as seen in Fig. 3. Theorem 4 follows our intuition that when the channel itself does not cause any inter-subcarrier interference due to the same inter-subcarrier spacing as in point-to-point communication situations, intentionally induced inter-subcarrier interference by non-trivial GFDM filtering will not be beneficial for SNR and hence for the rate. However, it will be shown later that even in the linear receiver case, SC-FDM is not optimal and non-trivial GFDM filtering enabling a countermeasure against channel-made inter-subcarrier interference is actually beneficial for the rate when there exists channel-made inter-subcarrier interference due to CFO as in uplink network situations.

IV. Filter Design Examples

In this section, we provide two design examples for GFDM. The first design goal is to minimize the OOB radiation and the second is to maximize the rate under CFO.

A. Design for OOB Radiation Minimization

OOB radiation minimization is one of the major issues in MC communication. Especially, in asynchronous bursty transmission of MTC or IoT data based on subcarrier modulation, synchronization required for waveform orthogonality is difficult to achieve and thus the spectral leakage of the waveform itself should be low not to significantly interfere with the data at different subcarriers [1].

For OOB radiation minimization, we first need to express the PSD of the continuous-time transmit signal generated from the discrete-time signal $x[n]$ as a function of the filter coefficients $\gamma_0, \cdots, \gamma_{2M-1}$. From (3), the discrete-time transmit signal $x[n]$ for one GFDM symbol interval can be rewritten as

$$x[n] = \sum_{k=0}^{K-1} e^{\iota 2\pi kn/K} \sum_{m=0}^{M-1} \tilde{g}[n-mK] s_{kM+m}, \tag{28}$$

where $\tilde{g}[n-mK]$ is given in terms of $\gamma_0, \cdots, \gamma_{2M-1}$ as

$$\tilde{g}[n-mK] = \frac{1}{\sqrt{NM}} \sum_{q=0}^{M-1} e^{\iota 2\pi (n-Km)q/N} \times (\gamma_q + e^{-\iota 2\pi n/K} \gamma_{M+q}). \tag{29}$$

(See Appendix for derivation of (29).) Let T_s be one subsymbol time interval corresponding to K time-domain samples and $T_b = MT_s$ be one GFDM symbol time interval. Under the assumption that a sample-level sinc interpolation filter is used, the discrete-time signal (28) is converted by changing n/K to t/T_s to the continuous-time signal for one GFDM symbol interval T_b as

$$x_{T_b}(t) = \sum_{k=0}^{K-1} e^{\iota 2\pi kt/T_s} \sum_{m=0}^{M-1} g_m(t) s_{kM+m}, \tag{30}$$

where $g_m(t)$ is given by (31), shown at the bottom of the page. Note that by sampling the continuous-time signal $x_{T_b}(t)$ in (30) at the sampling points $t = nT_c$, where T_c is the sample or chip time interval (i.e., $T_c = T_b/N = T_s/K$), we have the discrete-time signal $x[n]$ in (28).

$x_{T_b}(t)$ is the continuous-time signal conveying N data subsymbols s_{kM+m} for one GFDM symbol interval. In actual data transmission, GFDM symbols are successively transmitted with each GFDM symbol carrying different and independent N data subsymbols s_{kM+m} at each time. That is, $x_{T_b}(t)$ is repeated for each GFDM symbol interval i with independent data subsymbols $s_{kM+m}[i]$ for each GFDM symbol interval i if the CP part is ignored for simplicity.† Thus, the overall continuous-time signal is a filtered output of independent N input data subsymbols s_{kM+m} entering the overall filter at each T_b, and this overall continuous-time signal is a cyclo-stationary random process [16]. Note that the PSD of the cyclo-stationary baseband signal $\sum_{m=0}^{M-1} g_m(t) s_{kM+m}$ is the same for all $k = 0, 1, \cdots, K-1$, and is given by [16, p. 573]

$$P_{BB}(f) = \frac{P_s}{T_b} \sum_{m=0}^{M-1} |G_m(f)|^2, \tag{32}$$

†When the CP part is considered, a similar derivation is obtained with an increased time interval including the CP portion for the same $g_m(t)$. Note that $g_m(t)$ and $x_{T_b}(t)$ in (30) are periodic with period MT_s. See Section V.

where $G_m(f)$ is the Fourier transform of $g_m(t)$, given by

$$\begin{aligned} G_m(f) &= \int_{-\infty}^{\infty} g_m(t) e^{-\iota 2\pi ft} dt \\ &= \frac{1}{\sqrt{NM}} \sum_{q=0}^{M-1} e^{-\iota 2\pi mq/M} \left(\int_0^{MT_s} e^{\iota 2\pi t(q/(MT_s)-f)} \gamma_q dt \right. \\ &\quad \left. + \int_0^{MT_s} e^{\iota 2\pi t(q/(MT_s)-f-1/T_s)} \gamma_{M+q} dt \right) \\ &= \frac{1}{\sqrt{NM}} \sum_{q=0}^{M-1} e^{-\iota 2\pi mq/M} (e^{-\iota 2\pi T_b f} - 1) \left(\frac{\gamma_q}{\iota 2\pi (q/T_b - f)} \right. \\ &\quad \left. + \frac{\gamma_{M+q}}{\iota 2\pi (q/T_b - f - 1/T_s)} \right). \end{aligned} \tag{33}$$

Then, the overall PSD is given by

$$P(f) = \frac{P_s}{T_b} \sum_{k=0}^{K-1} P_{BB}\left(f - \frac{k}{T_s}\right), \tag{34}$$

since the overall signal $x_{T_b}(t)$ in (30) is the sum of the frequency-shifted versions $e^{\iota 2\pi kt/T_s} \sum_m g_m(t) s_{kM+m}$ of the baseband signals $\sum_m g_m(t) s_{kM+m}$, $k = 0, 1, \cdots, K-1$ and multiplication by $e^{\iota 2\pi kt/T_s}$ is shift in the frequency domain by k/T_s Hz.

The Fourier transform of a rectangular pulse with the time range $[0, MT_s]$ is a sinc function in the frequency domain which has the main lobe frequency range $[\frac{-1}{MT_s}, \frac{1}{MT_s}]$. Note from (31) that $g_m(t)$ is the sum of modulated rectangular pulses $\gamma_q e^{\iota 2\pi qt/(MT_s)}$ and $\gamma_{M+q} e^{\iota 2\pi t(q/(MT_s)-1/T_s)}$, $0 \le t \le MT_s$, $q = 0, \cdots, M-1$. Hence, $G_m(f)$ is the sum of the frequency-shifted sinc functions which have the main lobe range $[\frac{p-1}{MT_s}, \frac{p+1}{MT_s}]$, $p = -(M-1), \cdots, M-1$. Hence, $G_m(f)$ has the main lobe frequency range $f \in [-\frac{1}{T_s}, \frac{1}{T_s}]$ and $P_{BB}(f)$ has the same main lobe frequency range. Thus, the main lobe frequency range of the overall PSD $P(f)$ is given by $f \in [-\frac{1}{T_s}, \frac{K}{T_s}]$ since it is the sum of $P_{BB}(f - k/T_s)$, $k = 0, \cdots, K-1$.

Based on the PSD formula as a function of $\gamma_0, \cdots, \gamma_{2M-1}$ and the results in Section III, we now formulate optimal filter design problems for OOB radiation minimization as follows:

Problem 3 (OOB radiation minimization for GFDM-MF/SIC):

$$\begin{aligned} &\arg\min_{\boldsymbol{\gamma}} \max_{f \in [\frac{1}{T_s}, \infty)} P\left(-\frac{1}{T_s} - f\right) + P\left(\frac{K}{T_s} + f\right) \\ &\text{s.t.} \sum_{m=0}^{2M-1} |\gamma_m|^2 = M. \end{aligned} \tag{35}$$

In the MF/SIC receiver case, no rate constraint is applied since any filter satisfying the power constraint does not cause

$$g_m(t) = \begin{cases} \dfrac{1}{\sqrt{NM}} \displaystyle\sum_{q=0}^{M-1} e^{-\iota 2\pi mq/M} e^{\iota 2\pi qt/(MT_s)} (\gamma_q + e^{-\iota 2\pi t/T_s} \gamma_{M+q}), & 0 \le t \le T_b\,(= MT_s), \\ 0, & t \notin [0, T_b]. \end{cases} \tag{31}$$

a rate loss if ideal SIC on top of the MF receiver is assumed. However, in the linear receiver case a rate constraint should be included in the optimization since the OOB-optimal filter is not the rate-optimal filter in general.

Problem 4 (OOB radiation minimization for GFDM-ZF):

$$\begin{aligned}&\arg\min_{\boldsymbol{\gamma}} \max_{f\in[\frac{1}{T_s},\infty)} P\left(-\frac{1}{T_s}-f\right)+P\left(\frac{K}{T_s}+f\right)\\ &\text{s.t.} \sum_{m=0}^{2M-1}|\gamma_m|^2=M\\ &\quad R_{ZF}(\boldsymbol{\gamma})\geq(1-\eta)N\log(1+P_s/\sigma_n^2),\end{aligned} \tag{36}$$

where $\eta\in[0,1]$ is the allowed rate loss factor compared to the maximum possible rate and $R_{ZF}(\boldsymbol{\gamma})$ is provided in Theorem 2.

In Problems 3 and 4, $1/T_s$, which is the spacing between two adjacent subcarriers, is selected for the transition bandwidth from the passband to the stopband, but a different value can be used. In the case of the MMSE receiver, the same problem can be formulated as Problem 4 with $R_{ZF}(\boldsymbol{\gamma})$ replaced by $R_{MMSE}(\boldsymbol{\gamma})$ given in Theorem 3. Numerical results on the design by Problems 3 and 4 are provided in Section VI-A.

B. Design for Rate Maximization in General Channels with CFO

In section III-B, it is shown that the Dirichlet filter (i.e., SC-FDM) is rate-optimal for GFDM with the linear ZF or MMSE receiver in the AWGN channel case with no CFO. However, this is not valid in general channels especially when the channel is perturbed by CFO. In this subsection, we provide the second design example of maximizing the transmission rate in an uplink scenario with CFO.

In the uplink GFDM case, we need to change the system model considered in Section II. In the uplink GFDM case, we have simultaneously transmitting K users with independent local oscillators (LOs) and a common receiver with a common LO in the network, and each user is allocated to one subcarrier carrying M subsymbols. The transmit data of user k is $\mathbf{s}_k$, and the transmit signal vector of user k with size $N+N_{cp}$ samples is given by

$$\bar{\mathbf{x}}_k=\boldsymbol{\Omega}_t\mathbf{W}_N^H\mathbf{P}_k\boldsymbol{\Gamma}\mathbf{R}\mathbf{W}_M\mathbf{s}_k, \tag{37}$$

where $\boldsymbol{\Omega}_t=\left[[\mathbf{0}\ \mathbf{I}_{N_{\rm cp}}]^T\ \mathbf{I}_N\right]^T$ is the CP addition matrix at the transmitter. The transmit signal of user k propagates through an FIR channel $\mathbf{h}_k=[h_k[0],\cdots,h_k[N_{cp}-1]]^T$ to reach the common receiver. In general, there exists CFO for each user k because of the discrepancy between the LO frequency of each user used in upconversion and the LO frequency of the common receiver used in downconversion. Let $\epsilon_k=\frac{\hat{f}_k-f_k}{\Delta f}$ be the CFO of user k, where $\hat{f}_k$, f_k, and Δf are the estimated carrier frequency of user k, the original transmit carrier frequency of user k, and the frequency spacing of two adjacent subcarriers, respectively. The impact of CFO on the baseband model is implemented simply by multiplying the diagonal CFO matrix $\bar{\boldsymbol{\Pi}}(\epsilon_k)=\mathrm{diag}(e^{-\iota 2\pi\epsilon_k N_{cp}},\cdots,e^{-\iota 2\pi\epsilon_k},1,\cdots,e^{\iota 2\pi\epsilon_k(N-1)})$ to the baseband channel output $\mathbf{h}_k^T*\bar{\mathbf{x}}_k^T$ of user k [17, eq. 4]. Thus, the received signal of GFDM with CFO after CP removal and DFT is expressed as

$$\begin{aligned}\mathbf{y}_{CFO}&=\sum_{k=0}^{K-1}\mathbf{W}_N\boldsymbol{\Pi}(\epsilon_k)\boldsymbol{\Omega}_r\bar{\mathbf{H}}_k\boldsymbol{\Omega}_t\mathbf{W}_N^H\mathbf{P}_k\boldsymbol{\Gamma}\mathbf{R}\mathbf{W}_M\mathbf{s}_k+\mathbf{n},\\ &=\sum_{k=0}^{K-1}\mathbf{D}_k\boldsymbol{\Lambda}_k\mathbf{P}_k\boldsymbol{\Gamma}\mathbf{R}\mathbf{W}_M\mathbf{s}_k+\mathbf{n},\end{aligned} \tag{38}$$

where $\bar{\mathbf{H}}_k$ is the $(N+N_{\rm cp})\times(N+N_{\rm cp})$ Toeplitz channel filtering matrix for user k with $[\mathbf{h}_k^T\ \mathbf{0}^T]^T$ as the first column, $\boldsymbol{\Omega}_r=[\mathbf{0}\ \mathbf{I}_N]$ is the CP removal matrix, $\boldsymbol{\Pi}(\epsilon_k)$ is the lower-right $N\times N$ submatrix of $\bar{\boldsymbol{\Pi}}(\epsilon_k)$, $\mathbf{D}_k=\mathbf{W}_N\boldsymbol{\Pi}(\epsilon_k)\mathbf{W}_N^H$, and $\boldsymbol{\Lambda}_k=\mathbf{W}_N\boldsymbol{\Omega}_r\bar{\mathbf{H}}_k\boldsymbol{\Omega}_t\mathbf{W}_N^H$. The $N\times N$ matrix $\mathbf{D}_k$ with elements $[\mathbf{D}_k]_{i,j}=\frac{\sin\pi(N\epsilon_k-(i-j))}{\sin(\epsilon_k-(i-j)/N)}e^{\pi(N-1)(\epsilon_k-(i-j)/N)}$ of the noncentered Dirichlet kernel [17] is not diagonal with $\epsilon_k\neq 0$ and induces inter-subcarrier interference. The received signal $\mathbf{y}_{CFO}$ in (38) can be rewritten as

$$\mathbf{y}_{CFO}=\boldsymbol{\Psi}\mathbf{s}+\mathbf{n}, \tag{39}$$

where $\boldsymbol{\Psi}=[\boldsymbol{\Psi}_1\mathbf{F},\cdots,\boldsymbol{\Psi}_K\mathbf{F}]$ and $\boldsymbol{\Psi}_k=\mathbf{D}_k\boldsymbol{\Lambda}_k\mathbf{P}_k$.

We assume that full channel state information (CSI) is available at both the transmitters[‡] and the receiver and the ZF receiver is used, and consider two cases regarding the knowledge of the CFO values $\{\epsilon_1,\cdots,\epsilon_K\}$. First, we assume that the CFO values are known to the receiver. In this case, perfect ZF processing can be performed, i.e.,

$$\hat{\mathbf{s}}=\boldsymbol{\Psi}^{-1}\mathbf{y}_{CFO}=\mathbf{s}+\boldsymbol{\Psi}^{-1}\mathbf{n}, \tag{40}$$

and the corresponding sum rate is given by

$$R_{ZF,CFO}(\boldsymbol{\gamma},\boldsymbol{\epsilon})=\sum_{n=0}^{N-1}\log\left(1+\frac{P_s/\sigma_n^2}{[(\boldsymbol{\Psi}^H\boldsymbol{\Psi})^{-1}]_{n,n}}\right), \tag{41}$$

where $\boldsymbol{\epsilon}=[\epsilon_0,\cdots,\epsilon_{K-1}]$. Note that in this case there is no inter-subcarrier interference as seen in (40), and the sum rate in (41) assumes that the receiver knows all CFO values $\boldsymbol{\epsilon}=[\epsilon_0,\cdots,\epsilon_{K-1}]$ because the ZF receiver $\boldsymbol{\Psi}^{-1}$ requires the CFO information. Note that $\{\epsilon_1,\cdots,\epsilon_K\}$ are the residual CFO after carrier recovery and hence, identifying the (residual) CFO values $\{\epsilon_1,\cdots,\epsilon_K\}$ at the receiver may not be easy. Thus, a more practical assumption is that the receiver skips extracting the exact (residual) CFO information and simply uses the nominal ZF receiver $\hat{\boldsymbol{\Psi}}^{-1}$, where $\hat{\boldsymbol{\Psi}}=[\hat{\boldsymbol{\Psi}}_1\mathbf{F},\cdots,\hat{\boldsymbol{\Psi}}_K\mathbf{F}]$ and $\hat{\boldsymbol{\Psi}}_k=\boldsymbol{\Lambda}_k\mathbf{P}_k$ with the assumption $\mathbf{D}_k=\mathbf{I}$. The nominal ZF receiver output is given by

$$\hat{\mathbf{s}}=\hat{\boldsymbol{\Psi}}^{-1}\boldsymbol{\Psi}\mathbf{s}+\hat{\boldsymbol{\Psi}}^{-1}\mathbf{n}. \tag{42}$$

[‡]The required CSI at the transmitters (CSIT) is the frequency-domain channel response values of $\boldsymbol{\Lambda}_k$ corresponding to the nonzero part of $\mathbf{P}_k$ from each user. In most transmit signal design to exploit the channel, CSIT is assumed, e.g., in MIMO precoding. CSI at the receiver (CSIR) is anyway necessary for coherent decoding. One way to resolve the CSIT issue is that the receiver (the base station) with CSIR designs the GFDM filter and feedbacks the GFDM filter information to the transmitters (user equipments) through some control channel as in codebook-based MIMO precoding.

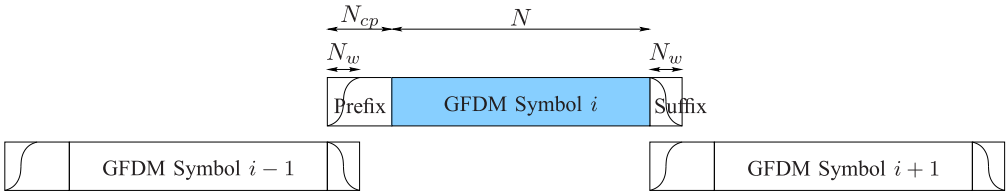

Fig. 1. Windowing with prefix and suffix [19].

Note that the nominal ZF induces inter-subcarrier interference, the SINR of the n-th subsymbol of $\hat{\mathbf{s}}$ is given by

$$\mathrm{SINR}_n^{\widehat{ZF}} = \frac{|[\hat{\mathbf{\Psi}}^{-1}\mathbf{\Psi}]_{n,n}|^2 P_s}{\sum_{i=0,i\neq n}^{N-1} |[\hat{\mathbf{\Psi}}^{-1}\mathbf{\Psi}]_{n,i}|^2 P_s + |[\hat{\mathbf{\Psi}}^{-1}]_{n,n}|^2 \sigma_n^2},$$

and the corresponding sum rate is given by

$$R_{\widehat{ZF},CFO}(\boldsymbol{\gamma},\boldsymbol{\epsilon}) = \sum_{n=0}^{N-1} \log\left(1+\mathrm{SINR}_n^{\widehat{ZF}}\right). \tag{43}$$

In this case, the rate-optimal filter design problem can be formulated as follows:

Problem 5 (Rate maximization for GFDM with nominal ZF with CFO):

$$\begin{aligned} \arg\min_{\boldsymbol{\gamma}} \quad & \mathbb{E}_{\boldsymbol{\epsilon}}\{R_{\widehat{ZF},CFO}(\boldsymbol{\gamma},\boldsymbol{\epsilon})\} \\ \text{s.t.} \quad & \sum_{m=0}^{2M-1} |\gamma_m|^2 = M. \end{aligned} \tag{44}$$

where $\mathbb{E}_{\boldsymbol{\epsilon}}$ is expectation over $\boldsymbol{\epsilon}$ with distribution $p(\boldsymbol{\epsilon})$.

In Problem 5, the cost function is the sum rate averaged over the CFO values since the CFO values are unknown and it is not desirable to design the filter for a specific set of CFO values. For the CFO distribution $p(\boldsymbol{\epsilon})$, we may consider a proper distribution such as a zero-mean Gaussian or uniform distribution. A closed-form solution to Problem 5 seems hard to obtain, but the problem can be solved numerically by approximating $\mathbb{E}_{\boldsymbol{\epsilon}}$ with the Monte Carlo method [18]. GFDM filter optimization for rate maximization under the MMSE receiver with CFO can be done in a similar way. Note that in Problem 5 the GFDM filter is optimized to maximize the data rate against CFO. It will be seen later in Section VI that the optimized GFDM filter in this way provides a non-trivial rate gain over SC-FDM especially at high SNR and the GFDM filtering is beneficial for the data rate even under linear receivers when the channel is perturbed by CFO.

V. Joint Design of GFDM Filter and Window

In this section, we consider the joint design of window and GFDM filter for the two design criteria in Section IV. For the windowing technique we consider windowing based on both prefix and suffix, as shown in Fig. 1 [19], [20]. In this method, the first $N_w(<N_{cp})$ samples $x_k[0], x_k[1], \cdots, x_k[N_w-1]$ of subcarrier k's signal $\mathbf{x}_k = \mathbf{W}_N^H \mathbf{P}_k \mathbf{\Gamma R W}_M \mathbf{s}_k$ are attached to the end of the vector $\mathbf{x}_k$ to yield a suffix of size N_w, while the last N_{cp} samples $x_k[N-N_{cp}], \cdots, x_k[N-1]$ of $\mathbf{x}_k$ are attached in the front of $\mathbf{x}_k$ just as a usual CP. Then, the first N_w samples of the CP and the last N_w suffix samples are symmetrically tapered with a proper window $\mathbf{w}^T = [w_1, \cdots, w_{N_w}, 1, \cdots, 1, w_{N_w}, \cdots, w_1]$ with $||[w_1, \cdots, w_{N_w}]||_2^2 = N_w/2$ for power constraint, the suffix of the previous symbol is overlapped with the first N_w samples of the prefix of the current symbol, as shown in Fig. 1, and finally the edge-overlapped GFDM symbols are transmitted. In this way, no additional time samples are required for windowing. At the receiver side, by taking only the N samples $y[0], y[1], \cdots, y[N-1]$ before the suffix part for each symbol, the same received signal model as in the case of no windowing can be obtained except the first $y[0], \cdots, y[N_w-1]$ samples may be corrupted by additive interference from the suffix part of the previous symbol. (If the possibility of the interference from the previous symbol needs to be eliminated completely, a CP of size $N_w + N_{cp}$ samples may be used with sacrificing the rate a bit.)

Now, consider the problem of rate maximization under CFO. If the aforementioned windowing and receiver-sampling technique is used, the inner received signal model is untouched. Hence, the rate optimization result in Section IV-B does not change, and the GFDM filter design for rate maximization under CFO and the window design can be separated. Under the goal of rate maximization under CFO, one reasonable approach is that we use the window to reduce the OOB radiation while using the rate-optimal GFDM filter against CFO perturbation proposed in Section IV-B to maximize the rate. In this case, the OOB-targeting window does not sacrifice the rate since the window does not affect the data rate. Here, we can adopt one of many windowing functions proposed for OOB reduction [19], [20].

On the other hand, under the goal of OOB emission reduction, the design of GFDM filter and window is intertwined. In the case of windowing with a prefix of N_{cp} samples and a suffix of N_w samples, the overall transmit signal is cyclo-stationary with period $T_{cp}+T_b$ and the constituent signal given by

$$x_{T_b'}(t) = \sum_{k=0}^{K-1} e^{\iota 2\pi k t/T_s} \sum_{m=0}^{M-1} w(t)\bar{g}_m(t) s_{kM+m}, \tag{45}$$

where $\bar{g}_m(t) = \frac{1}{\sqrt{NM}} \sum_{q=0}^{M-1} e^{-\iota 2\pi m q/M} e^{\iota 2\pi q t/(MT_s)} (\gamma_q + e^{-\iota 2\pi t/T_s}\gamma_{M+q})$ for $-T_{cp} \le t \le T_b + T_w$ and $\bar{g}_m(t) = 0$ for $t \notin [-T_{cp}, T_b+T_w]$, and $w(t) \neq 0$ only for $t \in [-T_{cp}, T_b + T_w]$ is the window function. Here, T_{cp} and T_w are the time intervals for N_{cp} and N_w samples, respectively. The baseband PSD of this cyclostationary signal is given by (32) with $G_m(f)$

replaced with $W(f) * \bar{G}_m(f)$, where $W(f)$ and $\bar{G}_m(f)$ are the Fourier transforms of $w(t)$ and $\bar{g}_m(f)$, respectively, and $*$ represents convolution. The overall PSD $P(f)$ is obtained by the K shifted sum of the baseband spectra as in (34). One suboptimal way to the joint design of GFDM filter and window for OOB emission minimization under the assumption of the MF/SIC receiver is that we simply design the GFDM filter to minimize OOB emission by solving Problem 3 with the modified PSD including the prefix and the suffix and additionally apply a known window function. However, this design does not have any optimality. To solve the joint optimization problem for OOB radiation minimization, we can adopt an alternating optimization technique widely used for joint optimization when direct joint optimization is difficult [21]. Applying this method, we propose the following algorithm for the joint design:

Algorithm 1: Initialize the window function $\mathbf{w}$ properly. First, optimize the GFDM filter as

$$\min_{\boldsymbol{\gamma}} \max_{f \in [\frac{1}{T_s}, \infty)} P\left(-\frac{1}{T_s} - f\right) + P\left(\frac{K}{T_s} + f\right) \tag{46}$$

under $\sum_{m=0}^{2M-1} |\gamma_m|^2 = M$ for the given window function. Then, for the obtained GFDM filter from (46), optimize the window function as

$$\min_{w_1, \cdots, w_{N_w}} \max_{f \in [\frac{N_{off}}{T_s}, \infty)} P\left(-\frac{1}{T_s} - f\right) + P\left(\frac{K}{T_s} + f\right) \tag{47}$$

under $||[w_1, \cdots, w_{N_w}]||_2^2 = N_w/2$. Iterate this procedure until convergence.

Note that we introduced the parameter $N_{off} \geq 1$ in (47). This is because typically windowing changes the slope of the spectral skirt of MC signals. Hence, we target enlarging the slope of the spectral decay by choosing the stop band away from the in-band with some large N_{off}. Although Algorithm 1 does not guarantee global optimality, it monotonically improves the performance at each iteration and a local optimality is guaranteed. The result of the joint design is provided in Section VI.

VI. Numerical Results

In this section, we provide some numerical results to validate our analysis and evaluate the performance of the proposed design methods. Since SC-FDM used for 4G uplink corresponds to GFDM with Dirichlet filters, SC-FDM as well as the previously considered RRC filter [10] were considered for the comparison baseline.

A. OOB Radiation Minimization

We evaluated the GFDM filter design method for OOB radiation minimization presented in Section IV-A. The considered GFDM parameters are $K = 60$, $M = 9$ ($N = KM = 540$), $\sigma_n^2 = 1$, and one subsymbol duration is normalized to be $T_s = 1$ sec (one GFDM symbol interval T_b is MT_s). First, we considered the case of no windowing with no CP and no suffix. We solved Problems 3 and 4 with $P_s = 1$ to obtain optimal GFDM filters for OOB radiation minimization in MF/SIC and ZF receiver cases, respectively, with the rates computed under the assumption of AWGN. The result is shown in Fig. 2 with $f = 0$ chosen to be the center of the signal bandwidth. For comparison, the PSD curves of SC-FDM and GFDM with RRC filters of roll-off factors $\alpha = 0.5$ and $\alpha = 0.9$ are included in Fig. 2. It is seen that the OOB-optimal GFDM filter targeting OOB radiation minimization without any constraint except the power constraint obtained by solving Problem 3 drastically reduces OOB radiation compared to SC-FDM, and the GFDM filter obtained by solving Problem 4 under the assumption of the ZF receiver with the 10 %, 30 %, and 50 % rate loss constraint compared to SC-FDM (i.e., $\eta = 0.1$, 0.3, and 0.5, respectively, in (36)) improves the OOB radiation performance compared to SC-FDM. However, in the latter case the OOB radiation improvement is not so drastic. It is also seen that GFDM with RRC filters with roll-off factors 0.5 and 0.9 yields slightly worse OOB performance than SC-FDM. Note in Fig. 2 that the decay rate of OOB radiation with respect to the frequency seems to be the same for all the considered GFDM filters including the OOB-optimal one obtained by solving Problem 3.

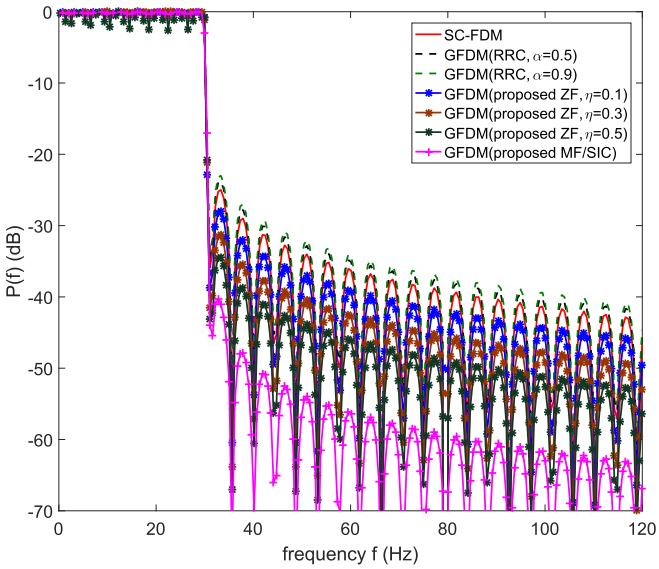

Fig. 2. OOB radiation: $K = 60$, $M = 9$, $T_s = 1$, $P_s = 1$, and $\sigma_n^2 = 1$.

Fig. 3 shows the rate performance corresponding to the result in Fig. 2 with the same system setup and SNR defined as P_s/σ_n^2. The GFDM filters were designed at 0 dB SNR (i.e., $P_s = \sigma_n^2 = 1$) but the SNR value was swept for the given GFDM filters. First, note that the rate performance of the GFDM filter obtained by solving Problem 3 assuming the MF/SIC receiver yields very poor rate performance when the corresponding GFDM filter is combined with the linear ZF receiver. Hence, in this case, SIC must be used for the desired rate performance. (When combined with the SIC receiver, it achieves the rate of SC-FDM as discussed in Section III-A. A practical combination may be that we first use the MMSE receiver and then use SIC.) In the case of the GFDM filter obtained by solving Problem 4 with $\eta = 0.1$ at 0 dB SNR under the assumption of the ZF receiver, there exists slight loss in the rate performance compared to SC-FDM. It is interesting to note that GFDM with RRC filters is good neither for the OOB performance nor for the rate

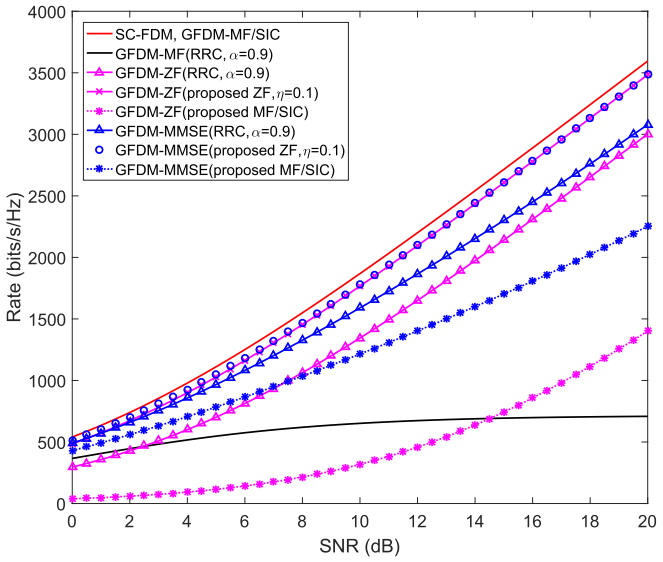

Fig. 3. Rate versus SNR.

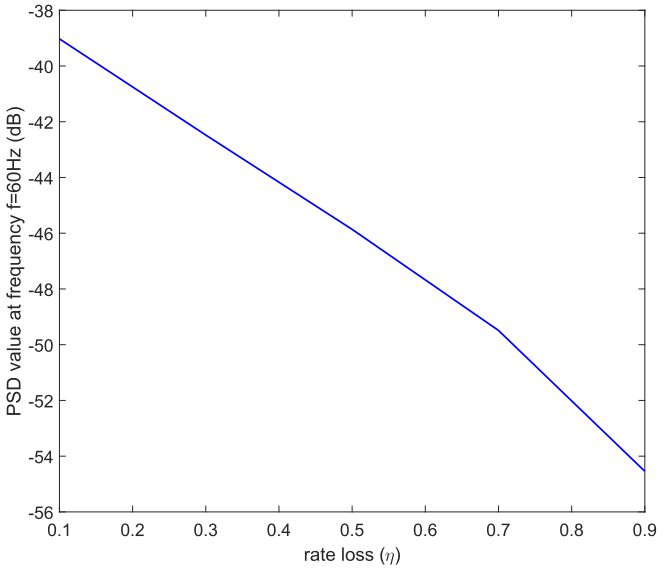

Fig. 4. Trade-off between the rate and OOB emission.

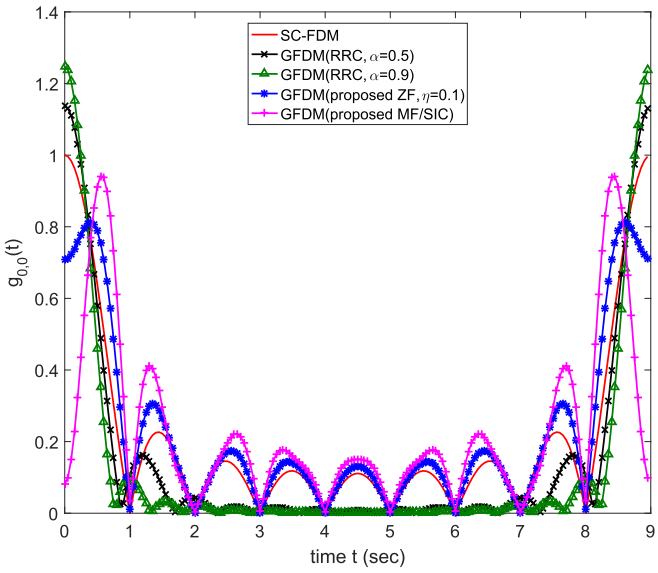

Fig. 5. Designed filter response in time domain.

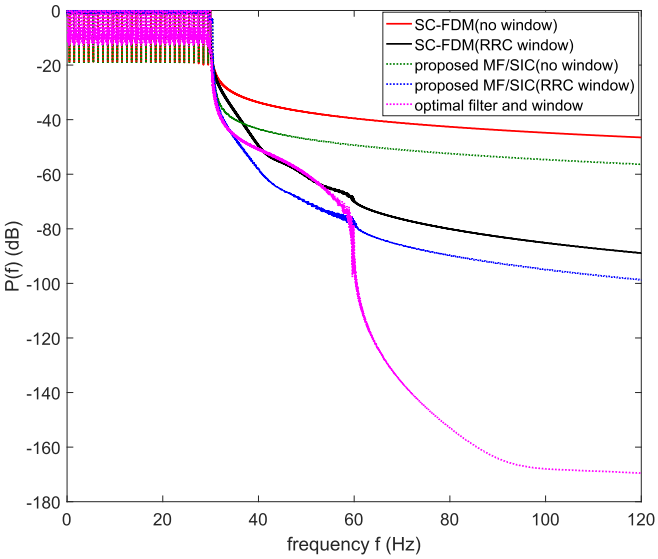

Fig. 6. OOB radiation: $K = 60$, $M = 9$, $T_s = 1$, $\sigma_n^2 = 1$, $P_s = 1$, $N_{cp} = 60$ (1/9=11.1%), and $N_w = 6$.

performance compared to SC-FDM. Hence, the RRC filter is not optimal in terms of rate-OOB emission trade-off. Note also that the rate performance of GFDM with a nontrival RRC filter and the MF receiver saturates quickly as SNR increases. Hence, the MF receiver is not a viable option for GFDM. Fig. 4 shows that OOB emission at $f = 60$ Hz for GFDM with the filter obtained from Problem 4 and the ZF receiver as a function of the rate loss constraint parameter η for the same setup as in Figs. 2 and 3. It is seen that the OOB performance monotonically improves as η increases, as expected. Indeed, in the linear receiver case, there exists a trade-off between the rate performance and the OOB radiation performance for the optimally designed GFDM filter Next, we considered the joint design of GFDM filter and window for OOB radiation minimization under the assumption of SIC at the receiver. To include windowing, we added $N_{cp} = 60$ samples in the front and $N_w = 6$ samples at the end of each GFDM symbol with the same parameters considered for Fig. 2, and used the windowing technique based on both prefix and suffix explained in Section V. We tried the two design methods mentioned in Section V. The first method is that we simply optimized the GFDM filter for OOB emission reduction by solving Problem 3 with the modified PSD including the prefix and the suffix, and applied a known window function. The second method is the joint optimization based on Algorithm 1. For Algorithm 1, we initialized the window with a rectangular window and chose $N_{off} = 60$. The result is shown inFig. 6. It is seen that with inclusion of prefix and suffix the gap between the proposed design and SC-FDM is reduced compared to Fig. 2 but there still exists significant improvement. It is also seen that with windowing additional OOB emission reduction is achieved. Note that the spectrum skirt obtained by

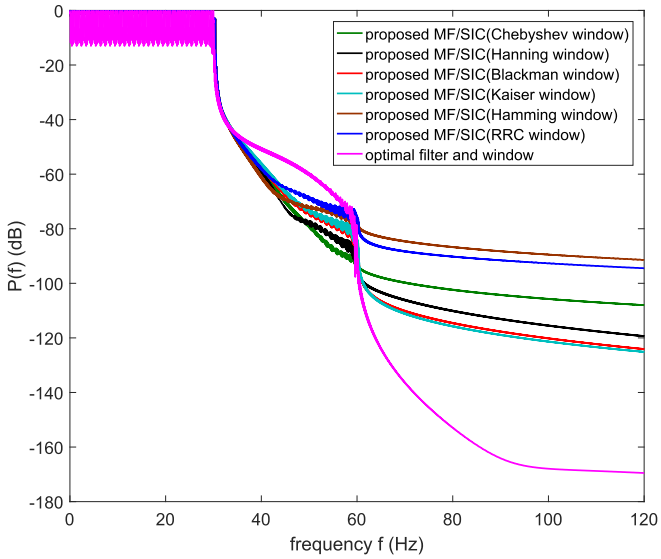

Fig. 7. OOB radiation with various windows.

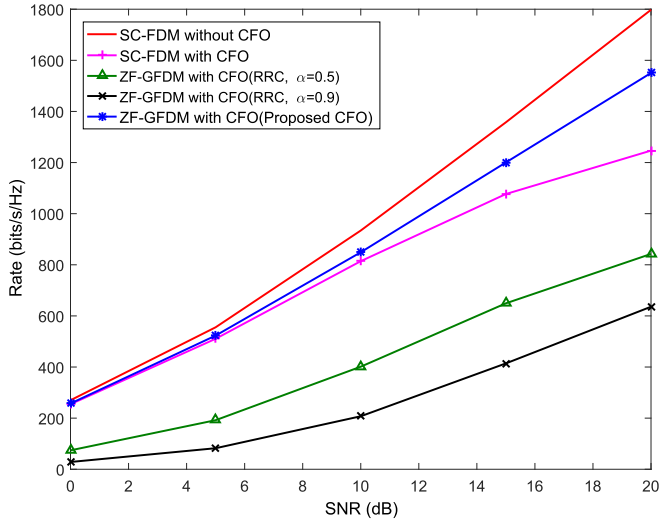

Fig. 8. Rate versus SNR: AWGN channel with CFO.

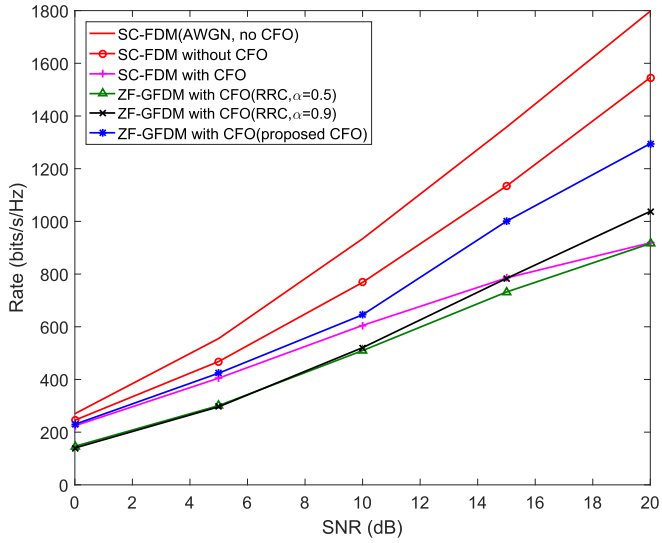

Fig. 9. Rate versus SNR: An LTE PB channel with CFO.

Algorithm 1 with $N_{off} = 60$ has a floor above the targeted cut-off frequency $f = 90$ Hz, which is a typical behavior of min-max optimization. (In Algorithm 1 the targeted cut-off frequency is $f = K/T_s + N_{off}/T_s$ Hz and K/T_s is shifted to $f = 30$ Hz in the figure although $K = 60$.) It is seen that the OOB emission reduction is far larger for the joint optimal design of GFDM filter and window than for the suboptimal method with the RRC window for $f \geq 60$. Fig. 7 shows the OOB radiation performance of various windows, Chebyshev window with the parameter $\alpha = 5$, Hanning window, Blackman window with the parameter $\alpha = 0.16$, Kaiser window with the parameter $\alpha = 2$, and Hamming window with the parameter $\alpha = 0.54$, combined with the GFDM filter obtained by solving Problem 3, together with that of the jointly optimized filter and window. (The parameter α for the corresponding window follows the conventional definition in the windowing literature.) Each window has $2N_w$ coefficients $[w_1, \cdots, w_{2N_w}]$ and is divided into the left $[1, N_w]$ part and the right $[N_w + 1, 2N_w]$ part which are applied to the beginning and end of one OFDM symbol, respectively. It is seen that Blackman and Kaiser windows yield good performance and the jointly optimized filter and window has far better than all other windows for $f \geq 60$.

Fig. 5 shows the time-domain filter magnitude response corresponding to Figs. 2 and 3. Note that the rate-optimal SC-FDM has one major peak, the OOB-optimal filter obtained by solving Problem 3 has two major peaks, and the filter obtained by solving Problem 4 seems a mixture of the two filter responses.

B. Rate Maximization under CFO

We considered an uplink GFDM network of $K = 6$ users with $M = 45$. The CFO ϵ_k for user k was generated according to the uniform distribution $\epsilon_k \sim \text{Unif}[-1/200, 1/200] = [-0.5\%, 0.5\%]$. (According to [22], the residual CFO is around $0.1\sim0.3\%$ relative to the carrier spacing.) We considered two channels with CFO: AWGN and the long term evolution (LTE) Pedestrian B (PB) channel with six non-zero multiple paths [23]. We considered the SNR range from 0 to 20 dB. To obtain a rate-optimal filter against CFO, we solved Problem 5 for each of the SNR values 0, 5, 10, 15, and 20 dB. The results are shown in Figs. 8 and 9. It is seen in Fig. 8 that in the AWGN with CFO, the performance of SC-FDM degrades from the case of no CFO and the proposed GFDM filter outperforms SC-FDM. It is also seen that the performance of the RRC filter is bad compared to other filters. In the general PB channel case, similar trends are seen in Fig. 9 In both cases, the performance gain of the proposed GFDM filter is large compared to SC-FDM at high SNR. This is because at high SNR the dominant factor for performance degradation is not noise but CFO. Hence, handling CFO properly with a well designed GFDM filter yields larger gain at high SNR.

Finally, we compared the OOB radiation of the GFDM filter used for Figs. 8 and 9, and the result is shown in Fig. 10. In the

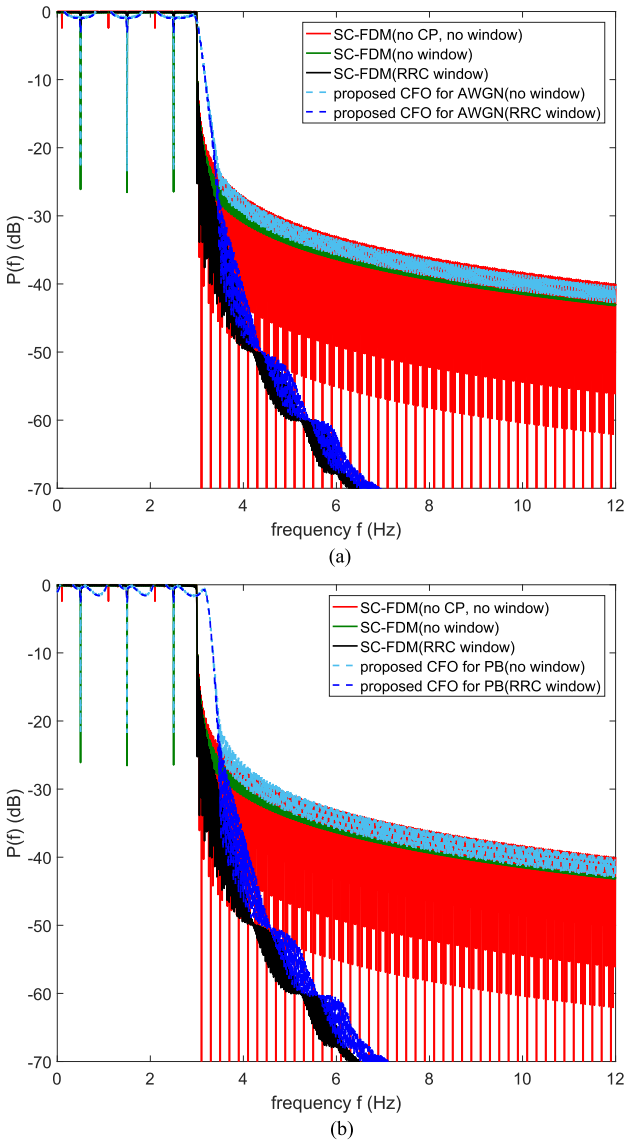

Fig. 10. PSD: (a) AWGN and (b) LTE PB channel.

AWGN channel case, it is seen that in the case of no window the OOB radiation decaying slope with respect to the frequency seems the same for SC-FDM and the proposed filter. In the windowing case, the spectrum skirt decreases significantly for both SC-FDM and the proposed GFDM filter used for Fig. 8. A similar behavior is seen in the LTE PB channel case, as shown in Fig. 10(b). Note that with the normalized $T_s = 1$, the subcarrier spacing is 1 Hz. The center frequencies of the six subcarriers ($K = 6$) are -2.5, -1.5, -0.5, 0.5, 1.5, and 2.5 Hz. In the case of SC-FDM, the waveform at each subcarrier occupies 1 Hz. In the case of GFDM with the repetition factor $L = 2$, on the other hand, the waveform at each subcarrier occupies 2 Hz. So, it is seen that the PSD of SC-FDM suddenly drops down at 3 ($= 2.5 + 1/2$) Hz and the PSD of GFDM with $L = 2$ extends to 3.5 ($= 2.5 + 2/2$) Hz. However, with windowing the window PSD envelope is dominant in both cases and the PSDs of both cases are very close beyond 3.5 Hz.

VII. Conclusion

We have considered optimal filter design for GFDM under the criteria of rate maximization and OOB emission minimization. In the case of rate maximization, we have shown that the Dirichlet filter is optimal in the AWGN channel with no CFO under linear receivers, but a properly designed non-trivial GFDM filter can yield better performance than the Dirichlet filter in general channels perturbed by CFO. In the case of OOB emission minimization, we have shown that drastic OOB reduction is possible by designing the GFDM filter properly under the assumption of MF/SIC receivers. Finally, we have shown that windowing can further enhance the performance when combined with a properly designed GFDM filter.

Appendix

Proof of Theorem 1: Note that

$$\mathbf{P}_k^T\mathbf{P}_i = \begin{cases} \mathbf{I}_{2M} & \text{if } k = i \,(\mathrm{mod}\, K), \\ \begin{bmatrix} \mathbf{0} & \mathbf{I}_M \\ \mathbf{0} & \mathbf{0} \end{bmatrix} & \text{if } k = i-1 \,(\mathrm{mod}\, K), \\ \begin{bmatrix} \mathbf{0} & \mathbf{0} \\ \mathbf{I}_M & \mathbf{0} \end{bmatrix} & \text{if } k = i+1 \,(\mathrm{mod}\, K), \\ \mathbf{0}_{2M\times 2M} & \text{otherwise}, \end{cases} \tag{48}$$

for $i = 0, \cdots, K-1$. From (11) and (48), we have

$$\begin{aligned} \mathbf{F}^H\mathbf{P}_k^T\mathbf{P}_i\mathbf{F} &= \mathbf{W}_M^H\mathbf{R}^T\mathbf{\Gamma}^*\mathbf{P}_k^T\mathbf{P}_i\mathbf{\Gamma}\mathbf{R}\mathbf{W}_M \\ &= \mathbf{W}_M^H[\mathbf{I}_M\ \mathbf{I}_M]\begin{bmatrix} \mathbf{\Gamma}^{(f)*} & \mathbf{0} \\ \mathbf{0} & \mathbf{\Gamma}^{(r)*} \end{bmatrix}\mathbf{P}_k^T\mathbf{P}_i\begin{bmatrix} \mathbf{\Gamma}^{(f)} & \mathbf{0} \\ \mathbf{0} & \mathbf{\Gamma}^{(r)} \end{bmatrix} \\ &\quad\cdot\begin{bmatrix} \mathbf{I}_M \\ \mathbf{I}_M \end{bmatrix}\mathbf{W}_M \\ &= \begin{cases} \mathbf{W}_M^H(\mathbf{\Gamma}^{(f)*}\mathbf{\Gamma}^{(f)} + \mathbf{\Gamma}^{(r)*}\mathbf{\Gamma}^{(r)})\mathbf{W}_M & \text{if } i = k, \\ \mathbf{W}_M^H(\mathbf{\Gamma}^{(r)*}\mathbf{\Gamma}^{(f)})\mathbf{W}_M & \text{if } i = k-1, \\ \mathbf{W}_M^H(\mathbf{\Gamma}^{(f)*}\mathbf{\Gamma}^{(r)})\mathbf{W}_M & \text{if } i = k+1, \\ \mathbf{0} & \text{otherwise}, \end{cases} \end{aligned} \tag{49}$$

where the mod notation is omitted. Then, from (17) we have

$$\begin{aligned} \hat{\mathbf{s}}_k &= \mathbf{F}^H\mathbf{P}_k^H\mathbf{P}\mathrm{diag}(\mathbf{F}, \cdots, \mathbf{F})\mathbf{s} + +\mathbf{F}^H\mathbf{P}_k^T\mathbf{W}_N\mathbf{n} \\ &= \sum_{i=0}^{K-1}\mathbf{F}^H\mathbf{P}_k^T\mathbf{P}_i\mathbf{F}\mathbf{s}_i + \mathbf{F}^H\mathbf{P}_k^T\mathbf{W}_N\mathbf{n} \\ &= \underbrace{\mathbf{W}_M^H(\mathbf{\Gamma}^{(f)*}\mathbf{\Gamma}^{(f)} + \mathbf{\Gamma}^{(r)*}\mathbf{\Gamma}^{(r)})\mathbf{W}_M}_{\mathbf{A}_k}\mathbf{s}_k \\ &\quad + \underbrace{\mathbf{W}_M^H(\mathbf{\Gamma}^{(r)*}\mathbf{\Gamma}^{(f)})\mathbf{W}_M}_{\mathbf{A}_{-k}}\mathbf{s}_{k-1} \\ &\quad + \underbrace{\mathbf{W}_M^H(\mathbf{\Gamma}^{(f)*}\mathbf{\Gamma}^{(r)})\mathbf{W}_M}_{\mathbf{A}_{+k}}\mathbf{s}_{k+1} + \mathbf{F}^H\mathbf{P}_k^T\mathbf{W}_N\mathbf{n}. \end{aligned} \tag{50}$$

Note that $\tilde{\mathbf{n}} \triangleq \mathbf{W}_N \mathbf{n} \sim \mathcal{CN}(0, \sigma_n^2 \mathbf{I}_N)$ since the DFT matrix $\mathbf{W}_N$ unitary and from (49)

$$\begin{aligned}\mathbf{F}^H \mathbf{P}_k^T \tilde{\mathbf{n}} &\sim \mathcal{CN}(\mathbf{0}, \sigma_n^2 \mathbf{F}^H \mathbf{P}_k^T \mathbf{P}_k \mathbf{F}) \\ &= \mathcal{CN}(\mathbf{0}, \sigma_n^2 \mathbf{W}_M (\mathbf{\Gamma}^{(f)*} \mathbf{\Gamma}^{(f)} + \mathbf{\Gamma}^{(r)*} \mathbf{\Gamma}^{(r)}) \mathbf{W}_M^H).\end{aligned} \tag{51}$$

Hence, the estimated signal of the m-th subsymbol of the k-th subcarrier is given by

$$\begin{aligned}\hat{s}_{kM+m} &= \sum_{p=0}^{M-1} [\mathbf{A}_k]_{m,p} s_{kM+p} + [\mathbf{A}_{-k}]_{m,p} s_{(k-1)M+p} \\ &+ [\mathbf{A}_{+k}]_{m,p} s_{(k+1)M+p} + [\mathbf{F}^H \mathbf{P}_k^T \tilde{\mathbf{n}}]_m \\ &= \sum_{p=0}^{M-1} \sum_{l=0}^{M-1} [\mathbf{W}_M^H]_{m,l} \Big([\mathbf{\Gamma}^{(f)*} \mathbf{\Gamma}^{(f)} + \mathbf{\Gamma}^{(r)*} \mathbf{\Gamma}^{(r)}]_{l,l} s_{kM+p} \\ &+ [\mathbf{\Gamma}^{(r)*} \mathbf{\Gamma}^{(f)}]_{l,l} s_{(k-1)M+p} \\ &+ [\mathbf{\Gamma}^{(f)*} \mathbf{\Gamma}^{(r)}]_{l,l} s_{(k+1)M+p} \Big) [\mathbf{W}_M]_{l,p} \\ &+ [\mathbf{F}^H \mathbf{P}_k^T \tilde{\mathbf{n}}]_m \\ &= \frac{1}{M} \sum_{p=0}^{M-1} \sum_{l=0}^{M-1} e^{\iota 2\pi (m-p) l/M} \Big[(|\gamma_l|^2 + |\gamma_{M+l}|^2) s_{kM+p} \\ &+ (\gamma_{M+l}^* \gamma_l) s_{(k-1)M+p} + (\gamma_l^* \gamma_{M+l}) s_{(k+1)M+p} \Big] \\ &+ [\mathbf{F}^H \mathbf{P}_k^T \tilde{\mathbf{n}}]_m. \end{aligned} \tag{52}$$

In (52), s_{kM+m} is the signal, s_{kM+p}, $\forall p \neq m$ is the interference from other subsymbols in the same subcarrier, $s_{(k-1)M+p}$ and $s_{(k+1)M+p}$, $\forall p$ are the interference from the adjacent subcarriers, and $[\mathbf{F}^H \mathbf{P}_k^T \tilde{\mathbf{n}}]_m$ is noise. Therefore, the signal power is $|\frac{1}{M} \sum_{l=0}^{M-1} (|\gamma_l|^2 + |\gamma_{M+l}|^2)|^2 P_s = P_s$ due to the constraint $\sum_{l=0}^{M-1} (|\gamma_l|^2 + |\gamma_{M+l}|^2) = M$, the interference power is $\frac{P_s}{M^2} \sum_{p \neq m, p=0}^{M-1} |\sum_{l=0}^{M-1} e^{\iota 2\pi (m-p) l/M} (|\gamma_l|^2 + |\gamma_{M+l}|^2)|^2 + \frac{2P_s}{M^2} \sum_{p=0}^{M-1} |\sum_{l=0}^{M-1} e^{\iota 2\pi (m-p) l/M} \gamma_l \gamma_{M+l}^*|^2 = a(\boldsymbol{\gamma}) P_s$, and the noise power is $\frac{\sum_{l=0}^{M-1} (|\gamma_l|^2 + |\gamma_{M+l}|^2)}{M} \sigma_n^2 = \sigma_n^2$ from (51) and the constraint $\sum_{l=0}^{M-1} (|\gamma_l|^2 + |\gamma_{M+l}|^2) = M$. Hence, the MF SINR is given by $\frac{P_s}{a(\boldsymbol{\gamma}) P_s + \sigma_n^2}$. ■

Proof of Theorem 2: From (20) the ZF equalizer after DFT is given by $\mathbf{B} := (\mathbf{P} \mathrm{diag}(\mathbf{F}, \cdots, \mathbf{F}))^{-1} \mathbf{\Lambda}_H^{-1}$ and hence the output SNR of the m-th subsymbol of the k-th subcarrier is given by [15]

$$\rho_{k,m,ZF}(\boldsymbol{\gamma}) = \frac{P_s / \sigma_n^2}{[\mathbf{B}\mathbf{B}^H]_{kM+m,kM+m}}. \tag{53}$$

The matrix $\mathbf{P} \mathrm{diag}(\mathbf{F}, \cdots, \mathbf{F}) = [\mathbf{P}_0 \mathbf{F}, \cdots, \mathbf{P}_{K-1} \mathbf{F}]$ in $\mathbf{B}$ can be written after some computation as

$$\begin{bmatrix} \mathbf{\Gamma}^{(f)} & \mathbf{\Gamma}^{(r)} & \cdots & \mathbf{0} \\ \mathbf{0} & \mathbf{\Gamma}^{(f)} & \ddots & \vdots \\ \vdots & \ddots & \ddots & \mathbf{\Gamma}^{(r)} \\ \mathbf{\Gamma}^{(r)} & \cdots & \cdots & \mathbf{\Gamma}^{(f)} \end{bmatrix} \mathrm{diag}(\mathbf{W}_M, \cdots, \mathbf{W}_M) \tag{54}$$

Then, $\mathbf{B} = \mathbf{W} \mathbf{C} \mathbf{\Lambda}_H^{-1}$, where $\mathbf{W} := \mathrm{diag}(\mathbf{W}_M^H, \cdots, \mathbf{W}_M^H)$ and

$$\mathbf{C} := \begin{bmatrix} \mathbf{\Gamma}^{(f)} & \mathbf{\Gamma}^{(r)} & \cdots & \mathbf{0} \\ \mathbf{0} & \mathbf{\Gamma}^{(f)} & \ddots & \vdots \\ \vdots & \ddots & \ddots & \mathbf{\Gamma}^{(r)} \\ \mathbf{\Gamma}^{(r)} & \cdots & \cdots & \mathbf{\Gamma}^{(f)} \end{bmatrix}^{-1}. \tag{55}$$

From the fact that $\mathbf{W}$ is a block diagonal matrix of repeated $\mathbf{W}_M^H$, the diagonal elements of $\mathbf{B}\mathbf{B}^H$ is given by

$$\begin{aligned}[\mathbf{B}\mathbf{B}^H]_{kM+m,kM+m} &= \sum_{i=0}^{N-1} |[\mathbf{B}]_{kM+m,i}|^2 \\ &= \sum_{i=0}^{N-1} |[\mathbf{W}\mathbf{C}\mathbf{\Lambda}_H^{-1}]_{kM+m,i}|^2 \\ &= \sum_{i=0}^{N-1} \left| \sum_{j=0}^{N-1} [\mathbf{W}]_{kM+m,j} [\mathbf{C}]_{j,i} [\mathbf{\Lambda}_H^{-1}]_{i,i} \right|^2 \\ &= \sum_{i=0}^{N-1} \left| \sum_{t=0}^{M-1} \frac{e^{\iota 2\pi m t/M}}{\sqrt{M}} \right. \\ &\quad \left. \times [\mathbf{C}]_{kM+t,i} [\mathbf{\Lambda}_H^{-1}]_{i,i} \right|^2. \end{aligned} \tag{56}$$

Using the fact that a block circulant matrix can be block-diagonalized by block DFT [24], we have

$$\mathbf{C}^{-1} = \begin{bmatrix} \mathbf{\Gamma}^{(f)} & \mathbf{\Gamma}^{(r)} & \cdots & \mathbf{0} \\ \mathbf{0} & \mathbf{\Gamma}^{(f)} & \ddots & \vdots \\ \vdots & \ddots & \ddots & \mathbf{\Gamma}^{(r)} \\ \mathbf{\Gamma}^{(r)} & \cdots & \cdots & \mathbf{\Gamma}^{(f)} \end{bmatrix} = \mathbf{U}\mathbf{D}\mathbf{U}^H, \tag{57}$$

where $\mathbf{U}$ is the unitary block DFT matrix given by

$$\mathbf{U} = \frac{1}{\sqrt{K}} \begin{bmatrix} \mathbf{I} & \mathbf{I} & \cdots & \mathbf{I} \\ \mathbf{I} & e^{\iota 2\pi/K} \mathbf{I} & \cdots & e^{\iota 2\pi (K-1)/K} \mathbf{I} \\ \vdots & \ddots & \ddots & \vdots \\ \mathbf{I} & e^{\iota 2\pi (K-1)/K} \mathbf{I} & \cdots & e^{\iota 2\pi (K-1)^2/K} \mathbf{I} \end{bmatrix}, \tag{58}$$

and

$$\mathbf{D} = \begin{bmatrix} \mathbf{d}_0 & \mathbf{0} & \cdots & \mathbf{0} \\ \mathbf{0} & \mathbf{d}_1 & \cdots & \mathbf{0} \\ \vdots & \ddots & \ddots & \vdots \\ \mathbf{0} & \cdots & \cdots & \mathbf{d}_{K-1} \end{bmatrix} \tag{59}$$

with $M \times M$ diagonal matrices

$$\mathbf{d}_l = \mathbf{\Gamma}^{(f)} + e^{\iota 2\pi l/K}\mathbf{\Gamma}^{(r)},\ l = 0, \cdots, K-1. \quad (60)$$

Hence, $\mathbf{C} = (\mathbf{U}\mathbf{D}\mathbf{U}^H)^{-1} = \mathbf{U}\mathbf{D}^{-1}\mathbf{U}^H$. By changing the variable i in (56) to $i = pM + q,\ p = 0, \cdots, K-1,\ q = 0, \cdots, M-1$, we have $[\mathbf{C}]_{kM+t,i}$ in (56) as

$$\begin{aligned}[\mathbf{C}]_{kM+t,pM+q} &= [\mathbf{U}\mathbf{D}^{-1}\mathbf{U}^H]_{kM+t,pM+q} \\ &= [\mathbf{U}(k,:)\mathbf{D}^{-1}\mathbf{U}(p,:)^H]_{t,q} \\ &= \frac{1}{K}\sum_{l=0}^{K-1} e^{\iota 2\pi(k-p)l/K}[\mathbf{d}_l^{-1}]_{t,q} \\ &= \delta_{t,q}\frac{1}{K}\sum_{l=0}^{K-1}\frac{e^{\iota 2\pi(k-p)l/K}}{\gamma_q + e^{\iota 2\pi l/K}\gamma_{M+q}}, \end{aligned} \quad (61)$$

where $\mathbf{U}(k,:)$ denotes the k-th block row of $\mathbf{U}$. By substituting (61) into (56), we have

$$[\mathbf{B}\mathbf{B}^H]_{kM+m,kM+m} = \sum_{p=0}^{K-1}\sum_{q=0}^{M-1}\left|\sum_{l=0}^{K-1}\frac{c_{k,p,q,l}}{\gamma_q + d_l\gamma_{M+q}}\right|^2, \quad (62)$$

where $c_{k,p,q,l}$ and d_l are defined in Theorem 2. The sum rate of GFDM-ZF is simply the sum of the N parallel Gaussian channels given by

$$R_{ZF}(\boldsymbol{\gamma}) = \sum_{k=0}^{K-1}\sum_{m=0}^{M-1}\log\left(1 + \rho_{k,m,ZF}(\boldsymbol{\gamma})\right). \quad (63)$$

Combining (53), (62) and (63) yields the desired result (21).

In the AWGN channel case of $\mathbf{\Lambda}_H = \mathbf{I}_N$, (62) becomes (64), shown at the bottom of the page, where step (a) is simple change of the summation order and step (b) is valid since $\sum_{p=0}^{K-1} e^{\iota 2\pi(k-p)(l-s)/K} = K$ if $l = s$ and $\sum_{p=0}^{K-1} e^{\iota 2\pi(k-p)(l-s)/K} = 0$ if $l \neq s$. Hence, the desired result (22) follows. ■

Remark 2 (Low-Complexity Computation of ZF Equalization): For ZF equalization, $\hat{\mathbf{s}} = (\mathbf{P}\mathrm{diag}(\mathbf{F}, \cdots, \mathbf{F}))^{-1}\mathbf{\Lambda}_H^{-1}\mathbf{W}_N\mathbf{y}$ should be computed as seen in (20). The left multiplication by $\mathbf{W}_N$ is simple N-point DFT, the left multiplication by $\mathbf{\Lambda}_H^{-1}$ is elementwise scaling since $\mathbf{\Lambda}_H$ is diagonal, and from (54), (55) and (57) $(\mathbf{P}\mathrm{diag}(\mathbf{F}, \cdots, \mathbf{F}))^{-1} = \mathbf{W}\mathbf{C} = \mathrm{diag}(\mathbf{W}_M^H, \cdots, \mathbf{W}_M^H)\mathbf{U}\mathbf{D}^{-1}\mathbf{U}^H$. Hence, the last step can easily be implemented by sequentially applying block IDFT $\mathbf{U}^H$, elementwise scaling $\mathbf{D}^{-1}$, block DFT $\mathbf{U}$ and finally K separate M-point IDFTs $\mathbf{W}_M^H$.

Proof of Theorem 3: From (12), (54) and (57), we have $\mathbf{\Phi} = \mathbf{W}_N^H\mathbf{C}^{-1}\mathbf{W}^H$, where $\mathbf{C}$ and $\mathbf{W}$ are defined in Proof of Theorem 2, and $\mathbf{\Phi}^H\mathbf{\Phi} = \mathrm{diag}(\mathbf{W}_M^H, \cdots, \mathbf{W}_M^H)\mathbf{U}\mathbf{D}^H\mathbf{D}\mathbf{U}^H\mathrm{diag}(\mathbf{W}_M, \cdots, \mathbf{W}_M)$. Let $\mathbf{V} := \mathrm{diag}(\mathbf{W}_M^H, \cdots, \mathbf{W}_M^H)\mathbf{U}$. Then, $\mathbf{V}$ is a unitary matrix since $\mathbf{U}$ and $\mathrm{diag}(\mathbf{W}_M, \cdots, \mathbf{W}_M)$ are unitary. Then,

$$\begin{aligned}\left(\mathbf{\Phi}^H\mathbf{\Phi} + \frac{\sigma_n^2}{P_s}\mathbf{I}_N\right)^{-1} &= \left(\mathbf{V}\mathbf{D}^H\mathbf{D}\mathbf{V}^H + \frac{\sigma_v^2}{\sigma_s^2}\mathbf{I}_N\right)^{-1} \\ &= \mathbf{V}\left(\mathbf{D}^H\mathbf{D} + \frac{\sigma_n^2}{P_s}\mathbf{I}_N\right)^{-1}\mathbf{V}^H. \end{aligned} \quad (65)$$

Therefore, the $(kM+m)$-th diagonal element of (65) is $\sum_{i=0}^{N-1}|[\mathbf{V}]_{kM+m,i}|^2[\mathbf{D}^H\mathbf{D} + \frac{\sigma_v^2}{P_s}\mathbf{I}]_{i,i}^{-1}$. Due to (59) and (60), changing the variable i with $i = lM + q,\ l = 0, \cdots, K-1,\ q = 0, \cdots, M-1$, we have

$$\left[\mathbf{D}^H\mathbf{D} + \frac{\sigma_n^2}{P_s}\mathbf{I}_N\right]_{lM+q,lM+q} = |\gamma_q + e^{\iota 2\pi l/K}\gamma_{M+q}|^2 + \frac{\sigma_n^2}{P_s}, \quad (66)$$

and from the definitions of $\mathbf{V}$ and $\mathbf{U}$ (see (58))

$$|[\mathbf{V}]_{kM+m,lM+q}|^2 = \left|\frac{1}{\sqrt{MK}}e^{-\iota 2\pi mq/M}e^{\iota 2\pi kl/K}\right|^2 = \frac{1}{N}. \quad (67)$$

Substituting (66) and (67) into (25) together with the fact $R_{MMSE}(\boldsymbol{\gamma}) = \sum_k\sum_m\log(1 + \rho_{k,m,MMSE}(\boldsymbol{\gamma}))$ yields the desired result (26). ■

Proof of Theorem 4: Consider the ZF case first. Note that the Dirichlet filter $\gamma_0 = \cdots = \gamma_{M-1} = 1$ and $\gamma_M = \cdots = \gamma_{2M-1} = 0$) satisfies the power constraint $\sum_{m=0}^{2M-1}|\gamma_m|^2 = M$. From (22), the corresponding rate is given by $N\log(1 + P_s/\sigma_n^2)$ because $\sum_{l=0}^{K-1}\sum_{q=0}^{M-1} 1/|\gamma_q + \gamma_{M+q}|^2 = N$ for the Dirichlet filter. Next, we show that N is the minimum value of the cost function $\sum_{l=0}^{K-1}\sum_{q=0}^{M-1}\frac{1}{|\gamma_q + d_l\gamma_{M+q}|^2}$ for all filters satisfying the power constraint. For this, we express the power constraint as $\sum_{q=0}^{M-1} g_q = M$, where $g_q := |\gamma_q|^2 + |\gamma_{M+q}|^2$. Then, the cost

$$\begin{aligned}[\mathbf{B}\mathbf{B}^H]_{kM+m,kM+m} &= \sum_{p=0}^{K-1}\sum_{q=0}^{M-1}\left|\frac{1}{\sqrt{M}}\frac{1}{K}\sum_{l=0}^{K-1}\frac{e^{\iota 2\pi(k-p)l/K}}{\gamma_q + d_l\gamma_{M+q}}\right|^2 \\ &= \frac{1}{MK^2}\sum_{p=0}^{K-1}\sum_{q=0}^{M-1}\sum_{l=0}^{K-1}\sum_{s=0}^{K-1}\frac{e^{\iota 2\pi(k-p)(l-s)/K}}{(\gamma_q + d_l\gamma_{M+q})(\gamma_q^* + d_s^*\gamma_{M+q}^*)} \\ &\overset{(a)}{=} \frac{1}{MK^2}\sum_{q=0}^{M-1}\sum_{l=0}^{K-1}\sum_{s=0}^{K-1}\frac{1}{(\gamma_q + d_l\gamma_{M+q})(\gamma_q^* + d_s^*\gamma_{M+q}^*)}\left(\sum_{p=0}^{K-1}e^{\iota 2\pi(k-p)(l-s)/K}\right) \\ &\overset{(b)}{=} \frac{1}{MK}\sum_{q=0}^{M-1}\sum_{l=0}^{K-1}\left|\frac{1}{\gamma_q + d_l\gamma_{M+q}}\right|^2. \end{aligned} \quad (64)$$

function is rewritten as

$$\sum_{l=0}^{K-1}\sum_{q=0}^{M-1}\frac{1}{|\gamma_q|^2+|\gamma_{M+q}|^2+2\mathrm{Re}(d_l\gamma_q^*\gamma_{M+q})} = \sum_{q=0}^{M-1}\sum_{l=0}^{K-1}\frac{1}{g_q+2\mathrm{Re}(d_l\gamma_q^*\gamma_{M+q})} \tag{68}$$

For each given q, $2\mathrm{Re}(d_l\gamma_q^*\gamma_{M+q})>-g_q$ for all $l=0,\cdots,K-1$ since $|\gamma_q+d_l\gamma_{M+q}|^2=g_q+2\mathrm{Re}(d_l\gamma_q^*\gamma_{M+q})>0$. Furthermore, for any (γ_q,γ_{M+q}) we have $\frac{1}{K}\sum_{l=0}^{K-1}2\mathrm{Re}(d_l\gamma_q^*\gamma_{M+q})=\frac{2}{K}\mathrm{Re}(\sum_{l=0}^{K-1}d_l\gamma_q^*\gamma_{M+q})=\frac{2}{K}\mathrm{Re}(\gamma_q^*\gamma_{M+q}\sum_{l=0}^{K-1}d_l)=0$ since $d_0=1,d_1=e^{\iota 2\pi/K},\cdots,d_{K-1}=e^{\iota 2\pi(K-1)/K}$ are located on the complex unit circle with equal spacing for $K>1$. Now applying Jensen's inequality, we have

$$\frac{1}{K}\sum_{l=0}^{K-1}\frac{1}{g_q+2\mathrm{Re}(d_l\gamma_q^*\gamma_{M+q})} \geq \frac{1}{g_q+\frac{1}{K}\sum_{l=0}^{K-1}2\mathrm{Re}(d_l\gamma_q^*\gamma_{M+q})}=\frac{1}{g_q}$$

since the function $\frac{1}{g_q+x}$ is convex for $x>-g_q$ and $\frac{1}{K}\sum_{l=0}^{K-1}2\mathrm{Re}(d_l\gamma_q^*\gamma_{M+q})=0$. Thus, (68) is lower bounded as

$$\sum_{q=0}^{M-1}\sum_{l=0}^{K-1}\frac{1}{g_q+2\mathrm{Re}(d_l\gamma_q^*\gamma_{M+q})} \geq K\sum_{q=0}^{M-1}\frac{1}{g_q} \geq \frac{N}{\frac{1}{M}\sum_{q=0}^{M-1}g_q}=N$$

by the Jensen's inequality since $1/x$ is convex for $x>0$ and $g_q>0$ for all q. Therefore, the GFDM-ZF rate of any filter satisfying the power constraint is less than or equal to $N\log(1+P_s/\sigma_n^2)$.

In the MMSE case, proof is similar to that of the ZF case. The Dirichlet filter with $\gamma_0=\cdots=\gamma_{M-1}=1$ and $\gamma_M=\cdots=\gamma_{2M-1}=0$ satisfying the power constraint $\sum_{m=0}^{2M-1}|\gamma_m|^2=M$ yields the rate $N\log(1+P_s/\sigma_n^2)$ because $D(\gamma)$ in (26) is $D(\gamma)=\frac{1}{1+\sigma_n^2/P_s}$ for the Dirichlet filter. Showing that $N\log(1+P_s/\sigma_n^2)$ is the best rate for GFDM with MMSE receivers is the same as that in the GFDM-ZF case. The cost function in Problem 2 is given by $\sum_{l=0}^{K-1}\sum_{q=0}^{M-1}\frac{1}{|\gamma_q+b_l\gamma_{M+q}|^2+\sigma_n^2/P_s}$. Applying the same techniques as in the proof of ZF case to the convex function $f(x)=\frac{1}{x+\sigma_n^2/P_s}$, we have

$$\sum_{l=0}^{K-1}\sum_{q=0}^{M-1}\frac{1}{|\gamma_q+b_l\gamma_{M+q}|^2+\sigma_n^2/P_s}\geq\frac{N}{1+\sigma_n^2/\sigma_s^2},\ \forall\boldsymbol{\gamma}.$$

Hence, $N\log(1+P_s/\sigma_n^2)$ is the best rate for GFDM with MMSE receivers. ■

Derivation of Eq. (29): From (12), (54) and (57), we have $\mathbf{x}=\mathbf{W}_N^H\mathbf{C}^{-1}\mathbf{W}^H\mathbf{s}=\mathbf{W}_N^H(\mathbf{U}\mathbf{D}\mathbf{U}^H)\mathrm{diag}(\mathbf{W}_M,\cdots,\mathbf{W}_M)\mathbf{s}$, where $\mathbf{U}$ and $\mathbf{D}$ are defined in (57), (58), (59) and (60), and hence $x[n]$ can be rewritten as (69) shown at the bottom of the page. For (69) and (70)–(72) as shown at the bottom of the page, we changed summation over $0,1,\cdots,N-1$ required for the n-th element of the product $\mathbf{W}_N^H(\mathbf{U}\mathbf{D}\mathbf{U}^H)$ to double sum over $p=0,\cdots,K-1$ and $q=0,\cdots,M-1$, and used the fact that $\mathrm{diag}(\mathbf{W}_M,\cdots,\mathbf{W}_M)$ is block-diagonal

$$x[n]=\sum_{p=0}^{K-1}\sum_{q=0}^{M-1}\sum_{k=0}^{K-1}\sum_{m=0}^{M-1}\frac{1}{\sqrt{N}}e^{\iota 2\pi n(pM+q)/N}[\mathbf{U}\mathbf{D}\mathbf{U}^H]_{pM+q,kM+q}\mathrm{diag}(\mathbf{W}_M,\cdots,\mathbf{W}_M)_{kM+q,kM+m}s_{kM+m} \tag{69}$$

$$=\sum_{p=0}^{K-1}\sum_{q=0}^{M-1}\sum_{k=0}^{K-1}\sum_{m=0}^{M-1}\frac{1}{\sqrt{N}}e^{\iota 2\pi n(pM+q)/N}\frac{1}{K}\sum_{l=0}^{K-1}e^{\iota 2\pi(p-k)l/K}(\gamma_q+e^{\iota 2\pi l/K}\gamma_{M+q})\frac{1}{\sqrt{M}}e^{-\iota 2\pi mq/M}s_{kM+m} \tag{70}$$

$$=\frac{1}{\sqrt{N}}\frac{1}{K}\frac{1}{\sqrt{M}}\sum_{k=0}^{K-1}\sum_{m=0}^{M-1}\sum_{q=0}^{M-1}\sum_{p=0}^{K-1}e^{\iota 2\pi n(pM+q)/N}e^{-\iota 2\pi mq/M}s_{kM+m}\sum_{l=0}^{K-1}(e^{\iota 2\pi(p-k)l/K}\gamma_q+e^{\iota 2\pi(p-k+1)l/K}\gamma_{M+q})$$

$$=\frac{1}{\sqrt{N}}\frac{1}{\sqrt{M}}\sum_{k=0}^{K-1}\sum_{m=0}^{M-1}\sum_{q=0}^{M-1}e^{\iota 2\pi n(kM+q)/N}e^{-\iota 2\pi mq/M}s_{kM+m}(\gamma_q+e^{-\iota 2\pi n/K}\gamma_{M+q}) \tag{71}$$

$$=\sum_{k=0}^{K-1}\sum_{m=0}^{M-1}e^{\iota 2\pi kn/K}\underbrace{\left[\frac{1}{\sqrt{K}}\frac{1}{M}\sum_{q=0}^{M-1}e^{\iota 2\pi(n-Km)q/N}(\gamma_q+e^{-\iota 2\pi n/K}\gamma_{M+q})\right]}_{g[(n-mK)_{\mathrm{mod}N}]}s_{kM+m}. \tag{72}$$

and $[\mathbf{UDU}^H]_{pM+q,kM+r} =$

$$\sum_{i=0}^{K-1}\sum_{j=0}^{M-1}[\mathbf{U}]_{pM+q,iM+j}[\mathbf{D}]_{iM+j,iM+j}[\mathbf{U}^H]_{iM+j,kM+r}$$

$$= \sum_{i=0}^{K-1}\sum_{j=0}^{M-1}\left[\frac{e^{\iota 2\pi pi/K}}{\sqrt{K}}\mathbf{I}\right]_{q,j}[\mathbf{D}]_{iM+j,iM+j}\left[\frac{e^{-\iota 2\pi ik/K}}{\sqrt{K}}\mathbf{I}\right]_{j,r}$$

$$= \sum_{i=0}^{K-1}\frac{e^{\iota 2\pi(p-k)i/K}}{K}[\mathbf{D}]_{iM+q,iM+q} \quad (q=j=r)$$

$$= \sum_{i=0}^{K-1}\frac{e^{\iota 2\pi(p-k)i/K}}{K}(\gamma_q + e^{\iota 2\pi i/K}\gamma_{M+q}).$$

(For $q \neq r$, $[\mathbf{UDU}^H]_{pM+q,kM+r} = 0$.) For (71) we used the facts that $\sum_{l=0}^{K-1} e^{\iota 2\pi(p-k)l/K} = K\delta_{p,k}$ and $\sum_{l=0}^{K-1} \mathbf{e}_k{}^{\iota 2\pi(p-k+1)l/K} = K\delta_{p,k-1}$. ■

REFERENCES

[1] G. Wunder *et al.*, "5GNOW: Non-orthogonal asynchronous waveforms for future mobile applications," *IEEE Commun. Mag.*, vol. 52, no. 2, pp. 97–105, Feb. 2014.

[2] R. W. Chang, "High-speed multichannel data transmission with bandlimited orthogonal signals," *Bell Syst. Tech. J.*, vol. 45, pp. 1775–1796, 1966.

[3] B. R. Saltzberg, "Performance of an efficient parallel data transmission system," *IEEE Trans. Commun.*, vol. 15, no. 6, pp. 805–811, Dec. 1967.

[4] B. L. Floch, M. Alard, and C. Berrou, "Coded orthogonal frequency division multiplex," *Proc. IEEE*, vol. 83, no. 6, pp. 982–996, Jun. 1995.

[5] W. Kozek and A. F. Molisch, "Nonorthogonal pulse shapes for multicarrier communications in doubly dispersive channels," *IEEE J. Sel. Areas Commun.*, vol. 16, no. 8, pp. 1579–1589, Oct. 1998.

[6] T. Strohmer and S. Beaver, "Optimal OFDM design for time-frequency dispersive channels," *IEEE Trans. Commun.*, vol. 51, no. 7, pp. 1111–1122, Jul. 2003.

[7] V. Vakilian, T. Wild, F. Schaich, S. ten Brick, and J.-F. Frigon, "Univalsal-filtered multi-carrier technique for wireless systems beyond LTE," in *Proc. Globecom*, Atlanta, GA, USA, Dec. 2013, pp. 223–228.

[8] M. Mukherjee, L. Shu, V. Kumar, P. Kumar, and R. Matam, "Reduced out-of-band radiation-based filter optimization for UFMC systems in 5G," in *Proc. Wireless Commun. Mobile Comput. Conf.*, Dubrovnik, Croatia, Aug. 2015, pp. 1150–1155.

[9] N. Michailow *et al.*, "Generalized frequency division multiplexing for 5th generation cellular networks," *IEEE Trans. Commun.*, vol. 62, no. 9, pp. 3045–3061, Sep. 2014.

[10] G. Fettweis, M. Krondorf, and S. Bittner, "GFDM - generalized frequency division multiplexing," in *Proc. Veh. Technol. Conf.*, Apr. 2009, pp. 1–4.

[11] N. Michailow, I. Gaspar, S. Krone, M. Lentmaier, and G. Fettweis, "Generalized frequency division multiplexing: Analysis of an alternative multi-carrier technique for next generation cellular systems," in *Proc. Int. Symp. Wireless Commun. Syst.*, Aug. 2012, pp. 171–175.

[12] I. Gaspar, N. Michailow, A. Navarro, E. Ohlmer, S. Krone, and G. Fettweis, "Low complexity GFDM receiver based on sparse frequency domain processing," in *Proc. Veh. Technol. Conf.*, Jun. 2013, pp. 1–6.

[13] E. Telatar, "Capacity of multi-antenna Gaussian channels," *Eur. Trans. Telecommun.*, vol. 10, pp. 585–595, Nov. 1999.

[14] H. Q. Ngo, E. G. Larsson, and T. L. Marzetta, "Energy and spectral efficiency of very large multiuser MIMO systems," *IEEE Trans. Comm.*, vol. 61, no. 4, pp. 1436–1449, Apr. 2013.

[15] Y. Jiang, M. K. Varanasi, and J. Li, "Performance analysis of ZF and MMSE equalizers for MIMO systems: An in-depth study of the high SNR regime," *IEEE Trans. Inf. Theory*, vol. 57, no. 4, pp. 2008–2016, Apr. 2011.

[16] J. Proakis and M. Salehi, *Fundamentals of Communication Systems*. Boston, MA, USA: Pearson, 2014.

[17] J. Lee, H.-L. Lou, D. Toumpakaris, and J. M. Cioffi, "Effect of carrier frequency offset on OFDM systems for multipath fading channels," in *Proc. Globecom*, Dallas, TX, USA, Dec. 2004, pp. 3721–3725.

[18] C. P. Robert and G. Casella, *Monte Carlo Statstical Methods*. New York, NY, USA: Springer, 2004.

[19] R. Prasad, *OFDM for Wireless Communications Systems*. Boston, MA, USA: Artech House, 2004.

[20] S. Plass, A. Dammann, S. Kaiser, and K. Fazel, *Multi-Carrier Systems and Solutions 2009*. New York, NY, USA: Springer, 2009.

[21] I. Gisszár and G. Tusnády, "Information geometry and alternating minimization procedures," *Statist. Decisions*, vol. 1, pp. 205–237, 1984.

[22] G. Wunder *et al.*, "5GNOW: Non-orthogonal, asynchronous waveforms for future mobile applications," *IEEE Commun. Mag.*, vol. 52, no. 2, pp. 97–105, Feb. 2014.

[23] 3GPP, "3GPP: Technical Specificiation Group Radio Access Network," 3GPP, France, Tech. Rep. 3GPP TR 25.890, May 2002.

[24] T. D. Mazancourt and D. Gerlic, "The inverse of a block-circulant matrix," *IEEE Trans. Antennas Propag.*, vol. 31, no. 5, pp. 808–810, Sep. 1983.

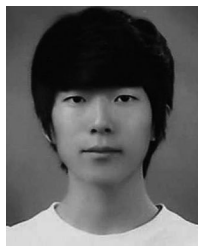

Seungyul Han (S'13) received the B.S. and M.S. degrees from the Korea Advanced Institute of Science and Technology (KAIST), Daejeon, South Korea, all in electrical engineering, in 2013 and 2016, respectively. He is currently working toward the Ph.D. degree at the KAIST. He is with the wireless information systems research group, KAIST. His research interests include signal processing for next generation communications.

Youngchul Sung (S'92–M'93–SM'09) received the B.S. and M.S. degrees from Seoul National University, Seoul, South Korea, in electronics engineering, in 1993 and 1995, respectively, and the Ph.D. degree in electrical and computer engineering from Cornell University, Ithaca, NY, USA, in 2005. He was a Senior Research Engineer at LG Electronics, Ltd., Seoul, South Korea from 1995 to 2000 and was a Senior Engineer at the Corporate R&D Center of Qualcomm, Inc., San Diego, CA, USA, from 2005 to 2007 with research focus on WCDMA. Since 2007, he has been on the Faculty of the Department of Electrical Engineering, KAIST, Daejeon, South Korea.

His research interests include signal processing for communications, statistical signal processing, asymptotic statistics, and information geometry. He is currently a Member of UNESCO/Netexplo University Advisory Board, Signal and Information Processing Theory and Methods (SIPTM) Technical Committee of Asia-Pacific Signal and Information Processing Association (APSIPA), Chair of the IEEE ComSoc Asia-Pacific Board MDC, and was an Associate Editor of the IEEE SIGNAL PROCESSING LETTERS from 2012 to 2014.

Yong H. Lee (S'80–M'84–SM'98) received the B.S. and M.S. degrees in electrical engineering from Seoul National University, Seoul, South Korea, in 1978 and 1980, respectively, and the Ph.D. degree in electrical engineering from the University of Pennsylvania, Philadelphia, USA, in 1984.

From 1984 to 1988, he was an Assistant Professor in the Department of Electrical and Computer Engineering, State University of New York, Buffalo, NY, USA. Since 1989, he has been in the Department of Electrical Engineering, South Korea Advanced Institute of Science and Technology, Daejeon, South Korea, where he is currently a Professor. He was the Provost from 2011 to 2013, the Dean of Engineering from 2005 to 2011, and the Head of Electrical Engineering from 2004 to 2005, all in KAIST. His research activities are in the area of communication signal processing, which includes interference management, resource allocation, synchronization, detection and estimation for multiple-input multiple-output, wireless communication systems including line-of-sight communications, and millimeter wave communication systems.